“Energy Relay Center” for doped mechano-luminescence materials: a case study on Cu or Mn doped CaZnOS

Bolong Huang[1]* and Dengfeng Peng[2] and Caofeng Pan[2]*

1. *Department of Applied Biology and Chemical Technology, The Hong Kong Polytechnic University, Hung Hom, Kowloon, Hong Kong SAR, China*
2. *Beijing Institute of Nanoenergy and Nanosystems, Chinese Academy of Sciences, Beijing 100083, P.R. China*

*Email: bhuang@polyu.edu.hk (BH); cfpan@binn.cas.cn (CP)

Abstract

We unraveled the mechanisms of transition metal doped mechano-luminescence materials through a case study of CaZnOS. We found the native point defect levels in Cu or Mn doped CaZnOS system acting as energy relay center for energy transfer of luminescence. Further with combination of native point defects levels discussed from previous work [***Phys. Chem. Chem. Phys.*** **18**, 25946 (2016)], we found the phosphor luminescence belongs to two different mechanisms. For Cu doping, it is a path via conduction band minimum to the Cu-t_{2g} level of 3d orbital localized in the band gap. The hole-drifting effect is found to support the reported red-shifting of emission. Both reversible and un-reversible mechanical quenching are attributed to the spatially separated electrons recombine the hole localized on Cu-t_{2g} level within the gap at levels below or above respectively. For Mn doping, it is a collaborative luminescence assisted by native point defects, and the excited states of Mn^{2+} is overlap with conduction band edge. The coexistence of Mn_{Zn} and Mn_{Ca} is confirmed but relatively low in Mn_{Ca}. The concentration quenching effect as well as the red-shift of absorption has shown a strong correlation with native point defects levels and relative position of $4T_1(^4G)$ state for both Mn_{Zn} and Mn_{Ca}. The further simplified approximation was used for modeling such concentration quenching effect.

Introduction

In the recent decade, mechanoluminescence (ML) has shown the great potential in energy conversion for applications of converting regular or irregular piezoelectricity, friction, stress/pressure in nature [1-6]. The related materials opened a wide range of channels for accommodating the external excitations, in manners of UV (ultraviolet) photo-irradiation, near-infra-red (NIR, e.g. 980 nm) photo-stimunlation, etc. The electron at the occupied trap level will be excited to a higher energy state near the conduction band (CB) edge or inside the CB region, which will be released backward to recombination with holes via either delocalized states in the CB, or inter-level transitions within the optical band gap area of host lattice. The energetic threshold for activating such electrons backward is relatively small in magnitudes of thermal perturbation or external mechano-stimulus, etc. The resulting visible luminescence for the electron-hole recombination at the activator site occurs in way of photon-emissions.

This class of luminescence materials has been reached to an accurate and flexible modulation stage that, the external energy has been characterized in terms of physical variables like mechanical stimulation. The applications of ML materials is promising in fields of either large human infrastructure constructions such as earth-quake prediction, stability test of large building or bridge, or electronics area such as hand-input oriented multi-touch technology in smartphone or other mobile devices combining with electronics magneto-opt-electronics [7-9]. More importantly, the demands in biological chemistry or biomedical area urge such ML materials to have stronger intensity, longer time and lower cost with flexible wavelength in persistent luminescence (phosphor luminescence) [10-20]. The demands are especially increasing nowadays in fields of wound inspection in subcutaneous tissue, or human friendly *invivo* or *invitro* imaging study for cancer tumor positioning or other related treatment.

However, as reviewed [12, 13, 21], this technique of phosphor luminescence property-modulation stays in the pattern of experimental attempts through the combination of host materials and rare-earth (RE) based activating dopant ion [22]. The non-RE doping such as transition metal or sp-block metal assisted luminescence are not well systematically explored and summarized. Moreover, large promising area of "*Biological Window*" for *invivo* imaging study of cancer tumor treatment is still leaving blank or with unknown theoretical guidance for mechanism study. An exact theoretical mechanism for persistent luminescence in terms of opto-electron excitation dynamics and charge carrier transfers is not clear. Moreover, the relationship between their native defect levels assisted electron transport and their upconverted persistent luminescence property is also still far from being well understood, especially at the electronic level. This blank in understanding not only hinders the process of designing new generations of persistent luminescence in the form of upconverted-mechano-persistent-luminescnece (UMPL), but also may affect the further development of existing technology, such as "*Inversed Design*" for specific luminescence materials on-demands in various fields. Further investigations to fill the gap are of great significance in the relevant science and related technological applications.

Recall from the pioneer work, Pan et al has already shown a feasible technology to achieve the RE-doped ML materials in both tribo-luminescence and phosphorescence, through a smart combination with single RE ion dopant [3, 6]. This trend is heading to a high color rendering excited by light-emitting-diode (LED) with Eu^{2+} activated by ML materials [23]. This success

arises because the well-known luminescence of f-block lanthanides has actually long been an important subject in optical applications and spectroscopy study [24-28]. The lanthanide rare-earth (RE) ions assisted phosphor luminescence technique has aroused tremendous interests in biological, chemical and physical applications, which play a leading role on modulating the luminescence properties[29]. From the previous work [30], we also proposed the concept of the upconverted-mechano-persistent-luminescence (UMPL), which is based on long-decay-time phosphorescence [12, 13, 21, 31], is challenged to downscale to smaller nanosized particle synthesis with faster charge response, lower cost and longer time for luminescence or mechanical signal image.

This left a question that, besides the f-block lanthanides, whether the d-block elements like transition metal (TM) ions (e.g. Mn or Cu) also have rich stories of manipulation on the ML intensity, color, and time-duration. Their mechano-stimunlus or doping concentration dependent ML seems to be also a hot topics for future prospective application or device manufacture. This confidence is sourced from the recent outcome reached by Xu et al [5, 32], who demonstrated a substantial leap in this field that some ML materials like oxy-sulfides can also be applied as persistent luminescence materials through transition metal doping, and with flexible color manipulations [33], especially towards to "*Biological Window*" wavelength region. This requires us not just only to understand the electronic structures that given by extrinsic doping, but also a high demanding to plot the photon-electron dynamic transitions based on the subtle energy conversion mechanisms during the process of persistent luminescence. Thus, to further on the study of the phosphor luminescence of ML materials, here we focus on two typical transition metal ion (Cu and Mn) doping effect and take the host lattice CaZnOS as example to illustrate the significance that native point defects assisted collaborative phosphor luminescence.

However, the interplay effect of different point defects levels is a significant issue. As known from previous works [30, 34-40], the native point defects in the host materials will not only produce a local lattice distortion or charge density anomalies, but also induce their unique localized electronic levels in the optical fundamental band gap in terms of either occupied or empty. In particular, the lattice distortions among these defect reactions support the electron transfer between different optical transition levels with exact amount of negative effective correlation energy ($-U_{eff}$) ideally. The native complementary charged point defects form a time-accumulated donor-acceptor pair (DAP) and produce band-like levels within the optical band gap of host materials, which is pinned by the $-U_{eff}$ effect along the closed cycle formed by zero-phonon-lines (ZPLs). Therefore, the stabilities and concentrations of native point defects from the host materials in persistent phosphors studies are quite important.

Another difficulty in experiment is that, thermal stimulated luminescence (thermal glow measurement, TSL) is used to be one of an effective technology to measure the trap depth and impurity levels of the persistent luminescence materials. However, the TSL is carried out under a varied temperature condition that may modify the original native point defect levels of host materials. This leads to a fact that the experimental observed trap level may not be the original trap levels as we expected. Moreover, the emission peaks measured from TSL experiments are usually too broad, and form into a defect bands instead of levels that influence the manipulation of luminescence accurately. Thus, these exact inter-levels of activators and traps within the

electronic structures suggested by the theoretical study will provide a reference for the selection towards the optimal performance [30, 34, 35, 41, 42].

There have been some questions raised by pioneer experiments regarding the TM-doped CaZnOS: (I) For the Cu-doping study by Xu et al [5], they found the red-shift of the emission peak from the phosphor luminescence. Meanwhile, recoverable, unrecoverable, and enhanced mechanical induced quenching effects have been found systematically. This indicates the participation of the native point defects during the process of the energy conversion for the luminescence. The Cu_{Zn}^{+} doping state has been induced for assistance of their schematic model. Thus, it is necessary to examine the single-particle levels of Cu substitutional doping in CaZnOS and subtle interplay between Cu doping level and native defect levels. (II) Differently, for the Mn-doping, Hintzen et al has initially studied the Mn^{2+} doping in CaZnOS and obtained an efficient red luminescence with a single fixed peak centered at 614 nm[43]. They deduced this red phosphor luminescence is actualized by Mn^{2+} optical transitions between the d-d transitions of Mn^{2+} itself in the lattice, and the crystal field effect also played an important contribution[43]. However, a following detailed and systematically asymptotic doping behavior studies provided the updated experimental observations and show the Mn^{2+} activated luminescence actually induces a red-shift of the phosphor luminescence starting from about 607 nm to 625 nm gradually with increased Mn doping concentration in CaZnOS[33]. The absorption edge is also red-shifted with increased doping concentration by diffuse reflection spectra measurement. Meanwhile, a 530 nm satellite emission is also found beside the 614 nm peak. Moreover, they found the Mn-doping concentration quenching effect, which is a uniformed decreased behavior of brightness/intensity of phosphor luminescence, decay time, and optical band gap width, with increase the Mn-doping concentration. This leads to a question that, if the luminescence only rely on the optical transitions between d-d levels of $4T_1(^4G)\rightarrow 6A_1(^6S)$, why it has concentration quenching effect. The optical band gap decreased with increasing doping amount of Mn, showing that it is also necessary to us to investigate the positions of $4T_1(^4G)$ level within the optical band gap. The x-ray diffraction (XRD) experiment on Mn-doped CaZnOS shows an evident shifting, leading us a question that whether a coexistence of Zn and Ca substituted Mn doping in the host lattice. Besides, based on the discussion by Hochheimer et al, there should have been a blue-shift effect among the transitions of $4T_1(^4G)\rightarrow 6A_1(^6S)$, instead of as-discovered red-shift in Mn^{2+} doped CaZnOS. Thus, crystal field effect is negligible or plays in a minor effect.

Proposed MQ modes by energy transfer:

According to the questions above, in the present work, we will interpret the phenomenon found in experiments based on previous calculations results and developed method to interpret the questions raised by experiments of Cu and Mn doping induced luminescence, which we think these belong to two different mechanisms for the phosphor luminescence in TM-doped CaZnOS. The as-discovered mechanical quenching effect will be discussed based on our calculated native point defect levels combined with Cu doping levels.

As illustrate in the Figure 1, CaZnOS presents three possible mechanical quenching effects: reversible mechanical quenching (R-MQ), un-reversible mechanical quenching (UR-MQ), and enhanced by mechanical quenching. For the ZnS system, there is a self-recoverable ML existing in ZnS but disappeared in ZnO due to the positions of different native point defect levels within the host band gap and acting the assistant role for energy transfer of luminescence.

In detail, the native electronic trap levels are accordingly divided by three classes. One is below the A-band as extra-deep donor trap levels, the second one is intermediated between D- and A- bands, and the third is staying at higher than the D-band. We here proposed that the CaZnOS normally have three mechanical quenching effects: reversible mechanical quenching (R-MQ), un-reversible-mechanical-quenching (UR-MQ), and enhanced effects. It is based on previous discussion that the native point defects widely separated within the band gap area. The donor (electronic) and acceptor (hole) trap levels are ranged from shallow to deep positions. The D- and A- bands are the transition levels of luminescence centers as discussed previously.

For the R-MQ, with loading applied, the first class electrons will be excited to recombine the holes at the A-band to recombine the localized holes forming a quenching effect. The luminescence intensity decreases. It will turn backward to the original electronic levels as the lower electronic level the more stability of electrons reaches in physical trend. Conversely, for the UR-MQ, the second class electrons move downward to recombine the holes at the A-band with mechanical stimulation. When the stimulation takes off, they would not fallback to the original levels as the energetically unfavorable since they meet a backward energy barrier. For the enhanced effect, the third class electronic levels are responsible. They can obtain enough high energy as excitations to jump into the delocalized conduction band and transport to the D-bands accordingly. This process is equivalent to increase the electronic concentrations for recombination in terms of emitting photons between D- and A- bands.

For the ZnS, the trap levels are mainly deep in the mid gap as discussed[44]. They mainly the second class type of traps with partially the first class participated. The luminescence will decay in form of UR-MQ when mechanical loading as excitation source.

For the ZnO, the electronic and hole levels are usually the second class dominated calculated by the calculations of one of our previous collaborators [45], and by Anderson and Van de Walle [46]. Only few of them will be excited by a substantial mechanical loading to the D bands, while most of them will downshift to the A-band to quench the luminescence. Thus, with mechanical loading, the luminescence intensity will hardly improve but decay quickly. Discussions are *vice-versa* for hole-process.

Calculation Setup

For a better understanding on the electronic contributions of the Cu and Mn doping in CaZnOS, we have carried out the First-Principles calculations based on the density functional theory (DFT) by CASTEP code [47], which basically inherited the calculation methods and setup used from the previous work [30]. We fixed the ground state relaxed lattice of CaZnOS geometrically reported from our previous work, where the lattice constant we got is a=b=3.758 Å, c=11.525Å, and the $\alpha=\beta=90°$, $\gamma=120°$, within $P6_3mc$ space group which is the same symmetry of wurtzite ZnO.

For the plan-wave basis set, it is highly recommend to carefully extending the cutoff energy to 850 eV for describing valence orbital components of Ca^{2+}, Zn^{2+}, Mn^{2+}, and $Cu^{2+/+}$ as well as the strongly localized states induced by 2p orbitals of O^{2-} and 3p of S^{2-}. To guarantee the convergence and avoid the charge-spin out-sync sloshing induced by high-spin state of Mn^{2+} and

Cu^{2+} (or Cu+), we uniformly chose the ensemble DFT (EDFT) method of Marzari et al [48]. The convergence tolerance of total energy calculations is set to no higher than $5.0x10^{-7}$ eV per atom, and the optimizations of Hellmann-Feynman forces in defect calculations are accomplished to lower than the level of 0.01 eV/Å. The Baldereschi special k-point (¼, ¼, 0) [49] with Gamma-center-off was self-consistently selected. Regarding the geometry relaxation, the algorithm based on Broyden-Fletcher-Goldfarb-Shannon (BFGS) method has been used through all bulk and defect supercell calculations.

The electronic density of states has been simulated based on anisimov-type rotational invariant PBE+U calculations [50], since the PBE functional in DFT has been recognized to be reliable for structural relaxation and cell optimization of d or even f-orbital based solids [51-53], regardless whether ultrasoft or norm-conserving pseudopotentials. Therefore, it is a suitable way to keep consistency by aligning with our previous work[30]. Furthermore, for the rotational invariant U parameter, it has been self-consistently determined based on our previous methodology on the Hermitian type density matrix for both charge and potential diagonalization during the two-way crossover perturbation. This has works on oxides [35, 36, 52-54], sulfides [34], oxysulfides [30], and fluorides [55] by our efforts and collaborations. Through our self-consistently determination process[34-37, 52-54], the on-site Hubbard U parameters for 3d of Ca and Zn are 2.50 eV, 13.45 eV, 2.87 eV for the 3p of S, and 3.44 eV for the 2p of the O, respectively. Moreover, the U_{3d} for Cu_{Zn} and Cu_{Ca} are self-consistently determined as 7.80 eV and 5.30 eV respectively, while 3.46 eV and 2.70 eV for U_{3d} for Mn_{Zn} and Mn_{Ca} in CaZnOS respectively.

It is worth to address that, to reduce the influence of the localized hole states produced by 2p orbitals of O sites and 3p of S sites, the self-consistently determined Hubbard U potentials is also applied on the O-2p orbitals and S-3p orbitals, which have been reached a consensus [56-59] in many oxides materials. Thus, it is necessary to consider both self-energy corrections on f- and p-orbitals for oxides [36, 37, 54]. By way of OPIUM code in generation with recent RRKJ optimization method [60], we "tailor-made" the norm-conserving pseudopotentials within the most popular KB (Kleinman-Bylander) projector framework [61], and the non-linear partial core corrections [62], which has been won the recognition through our theoretical development [36]. Especially for the pseudopotential of Cu, a valence configuration with ($3d^{10}$, $4s^{1}$) has been chosen for representing the neutral Cu atom. This has been successfully used by our work, for testing the deep hole trap levels induced by O-related native point defects states in Cu_2O system with a corrected band gap in agreement with experiments [52].

To calculate defect formation energy calculations at different charge states (q), we consider the overall supercell was established and remained constantly based on the ground state relaxed primitive cell, to avoid the thermodynamic effect of enthalpy changes by cell variations. The formation energy of a targeted defect (H_q) at the specific charge state q, can be described as a relation of the positions of Fermi energy (E_F) and the chemical potential $\Delta\mu$ of species of defects α, which is shown as follow:

$$H_q(E_F,\mu)=\left[E_q-E_H\right]+q\left(E_V+\Delta E_F\right)+\sum_{\alpha} n_\alpha\left(\mu_\alpha^0+\Delta\mu_\alpha\right), \quad (1)$$

The above E_q and E_H are the total energy of a relaxed defective lattice in charge state q and an ideal host lattice at the ground-state, respectively. The ΔE_F in Eq. (4) is the change of Fermi

energy with respect to the valence band maximum (VBM, E_V=0), and n_α is the number of atoms of constituent element α chosen as targeted defect sites, then the μ_α^0 is referenced chemical potential, based on the method used by the work of Zunger et al [63].

Results and discussion

Cu_{Zn} doping

Experimentally, two cation sites, Ca and Zn, are the possible center for Cu substitutional doping. Figure 2 (a) shows the partial density of states (PDOSs) of CaZnOS with Cu doped on Zn site (Cu_{Zn}), at three different charge states, 0, +1, and +2. We can treat it as [3S-Cu-O] for representing the local motif, and Cu site is 4-fold coordinated in tetrahedral configuration. We see that Cu_{Zn} provides deep hole trap center. As we can see, the localized defect levels are very different from the native V_{Zn} in CaZnOS from our previous work [30], But cation dopants with same ordinary charge states as the targeted substitution sites are usually the centers of localized hole traps is following the previous observations based on CaS system [34]. From the relaxed structure in neutral state, the Cu_{Zn}^{0} induces less lattice relaxations compared to the native cation vacancy defects as discussed previously. Three Cu-S bonds are 2.367 Å, 2.368 Å, and 2.376 Å respectively, which are shortened with only 0.1~0.2 Å. The Cu-O bond has the length of 1.881 Å compared to 1.914 Å from previous Zn-O bond. The PDOSs from Figure 2 (a) shows the localized hole state of Cu_{Zn}^{0} is 2.35 eV below the CB edge in spin-down. There are a few electronic states are staying at the VB edge. For the Cu_{Zn}^{+} state, there are extra hole states pushed out from the top of VB (VBM) in spin-down configuration, while the band tail like electronic states remained at the VB edge. The Cu_{Zn}^{+} also gives localized hole state with 2.57 eV below the CB edge, this shows a close agreement with the observed phosphorescence emission wavelength of 483 nm (2.56 eV in photon energy) from the experiment done by Xu et al [5]. Further on the 2+ state (Cu_{Zn}^{2+}), the localized hole states turn to be even shallow, with 2.67 eV far below the CB edge, and it is also showing a good agreement with experiment in wavelength of 464 nm compared to experimental 472 nm [5], with only a relative deviation of 2%. In ordinary cases, the optical transitions between 3d-4s orbital levels are parity forbidden. However, as shown from Figure 2 (a), the CB edge are consist of partial hybridized s and p orbitals that lowered down the restrictions of selection-rule, the optical transitions are accordingly allowed to carry on, this can be found in similar statement from Tanner's work [64]. Therefore, the optical transitions between such localized level and CB edge are implementable and parity allowed.

Figure 2 (b) shows the orbitals for localized gap levels that induced by the Cu_{Zn} in CaZnOS. We see that the localized hole states are usually occupying the hybridized $3d_z^2$ and $2p_z$ between Cu and O sites respectively, along the Cu-O bond direction. This scenario happens in three different charge states with different orbital expansion range in real space. While, in the +2 charge states (Cu_{Zn}^{2+}), an extra localized hole state is occupying the $3d_{xy}$ orbital and interacting the localized $3p_{x,y}$ of nearest neighboring S sites along the Cu-S bond direction. For the electronic states staying near the VB edge, as discussed above in Cu_{Zn} doped CaZnOS, they are all found to be delocalized $3p_x$ or $3p_y$ orbitals wide spread in the lattice. This indicates the Cu_{Zn} will release the out-shell valence electrons into Cu_{Zn}^{+} or Cu_{Zn}^{2+} state which will enter the valence band as a stable state versus the Fermi level (E_F). The electrons will be spread over in-plane $3p_x$ or $3p_y$ orbitals of S sites. We also see that the as-introduced localized hole states arises because of the correlations between partially occupied $3d^{10-\delta}$ ($0<\delta<1$) orbitals and 2p or 3p orbitals of O

and S sites. There is no perturbed hole states (PHS) next to the CB edge [65, 66]. The observed single localized hole level is different from the case of native point defect levels in other solid functional materials[30, 34-37].

The formation energy of Cu_{Zn} at 0, +1, and +2 is calculated and shown in Figure 2 (c). It is showing that the Cu_{Zn} has negative effective correlation energy (negative-U_{eff}) with -0.12 eV among three different charge states. This indicates an exothermal defect reaction process of $2Cu_{Zn}^{+} \rightarrow Cu_{Zn}^{0} + Cu_{Zn}^{2+}$ and nearly ESR silent or undetectable measurement on its practical doping concentrations. The related negative-U_{eff} is obtained through a process: $U_{eff}=[E_{form}(q=0)+E_{form}(q=+2)]-2E_{form}(q=+1)$, where the formation energy is obtained following the Equation (1) in the calculation setup. From the plot of formation energy versus the Fermi level (E_F), the negative-Ueff means the crossover point between curves of neutral and doubly positive Cu_{Zn}^{0} and Cu_{Zn}^{2+} will be found under the curve of singly positive Cu_{Zn}^{+} state.

Meanwhile, the concentration of Cu_{Zn}^{+} is relatively low compared to Cu_{Zn}^{0} and Cu_{Zn}^{2+}, but it can be temporarily formed in the host with short life-time by external UV photo-irradiation or other high-energy excitations. In fact, we further on high concentration Cu_{Zn} formation energy calculations within smaller CaZnOS supercell (2×2×2). The negative-U_{eff} turns to be more negative value of -0.25 eV, showing the physical chemistry trend that the Cu_{Zn}^{+} has intrinsically low concentration in CaZnOS. Therefore, it is show by our calculation that the discussed role of Cu_{Zn}^{+} in optical transitions process from the work by Xu et al may be temporarily formed due to UV irradiation [5].

Intrinsic formation of Cu_{Zn}^{+} in low concentration contributes another possible route for optical transition or an energy relay center as introduced by our previous work [34]. Such Cu_{Zn}^{+} level is thermodynamically unstable, and will experience the above reaction transition into Cu_{Zn}^{0} or Cu_{Zn}^{2+}. Besides, the neutral Cu doping state (Cu_{Zn}^{0}) in CaZnOS has energies of 2.96 eV and 0.99 eV under chemical potential of S-rich and Zn-rich limits respectively. The thermodynamic transition level (TTL) of Cu_{Zn} is E_V+0.125 eV for (0/2+) above the VBM (E_V for VBM). This implies that the Cu_{Zn} is an extra deep donor-like trap center. The extra deep donor level also indicates that the Cu_{Zn}^{0} will be the stable state in the band gap in relatively wide E_F range from E_V+0.125 eV (the TTL of (0/2+)) to E_V+3.9 eV (CB edge). Therefore, the relative position of TTL in the band gap for Cu_{Zn} is found to be in a good agreement with deduced schematic diagram by Xu et al [5], but it is transitions of (0/2+) according to our calculation.

Cu_{Ca} doping

We turn to look at the Cu_{Ca} doping in CaZnOS lattice, which is [3O-Cu-3S] as the local motif and 6-fold coordinated in distorted A7-like local structural configuration. As indicated in Figure 3 (a), the PDOS shows similar trend to the case of Cu_{Zn}. Among three different charge states, 0, +1, and +2, the localized hole states are all deep in the band gap of host lattice, as well as some electronic and hole band tail states at the VB edge near the E_F. In the relaxed neutral Cu_{Ca} doped structure, the Cu-O bond was shortened from 2.354 Å to 2.042 Å, while the Cu-S bond was prolonged to 3.223 Å compared to original Zn-O and Ca-S bond lengths in CaZnOS respectively. The PDOSs from Figure 3 (a) shows the localized hole state of Cu_{Ca}^{0} is 2.64 eV (470 nm) above the VBM in a close consistency with experimental 472 nm [5], and some shallow acceptor-like

states are sitting at the top of VB acting as VB band tail. For the Cu_{Ca}^{+} doping state, the hole-like VB band tail states turn to be more evident as 0.20 eV in difference compared to spin-up state. The energy interval between the localized mid-gap hole state and VB tail is 2.93 eV. For the Cu_{Ca}^{2+}, the localized hole state is 2.58 eV (481 nm) higher than the hole-like VB tail states (0.33 eV above the E_F), also close to the experimental 483 nm [5]. Based on the as-discussed localized hole levels of Cu_{Ca}, the optical transitions paths that match the experimental emission wavelength in phosphorescence are different from the case of Cu_{Zn} in CaZnOS. In Cu_{Ca} doping case, the optical transition is from the localized mid-gap hole to the VB tail state. While for Cu_{Zn}, it is from CB edge to mid-gap hole state.

As indicated in Figure 3 (b), the orbitals of localized levels induced by Cu_{Ca} are slightly different from the Cu_{Zn} in CaZnOS. This difference can be also found from our self-consistently determined on-site Coulomb potential Hubbard parameter for Cu (5.298 eV for Cu_{Ca} and 7.805 eV for Cu_{Zn} respectively). In Cu_{Ca}^{0} state, the deep localized hole state shows a single isolated $3d_z^2$ orbital from Cu dopant site. This indicates a potential weak interaction for Cu in 6-fold coordination [3S-Cu-3O] by substituting the original Ca site. Another localized hole state is staying at the CB edge with p-d orbital hybridization between Cu and three S sites in the plane of CaS sublattice of CaZnOS system. For the Cu_{Ca}^{+} state, the localized hole orbitals are evidently different from the neutral state. The localized mid-gap hole state is anisotropic and in $3d_z^2$ component configuration horizontally coupling with nearest neighboring O sites in CaO sublattice layer. Meanwhile, the other is sitting near the CB edge with more obvious hybridization between 3d and 2p orbitals of Cu and O respectively. The localized hole states orbitals in Cu_{Ca}^{2+} are rather similar to the neutral state with smaller range of isosurface of orbitals in real-space, denoting less localized holes nearby.

Figure 3 (c) shows the calculated formation energy of Cu_{Ca} at charge states of 0, +1, and +2. We see that the Cu_{Ca} cost more energy to be doped than Cu_{Zn}. This may arise because Cu has more similar ionic radius to the Zn compared to Ca in CaZnOS host lattice. It notes that the Cu_{Ca} in CaZnOS possesses positive effective correlation energy (positive-U_{eff}) with value of +0.81 eV for the defect reaction process of $2Cu_{Ca}^{+} \rightarrow Cu_{Ca}^{0} + Cu_{Ca}^{2+}$. It indicates an endothermal process for such reaction and Cu_{Ca}^{+} is supposed to be the dominant Ca substitutional doping state in the CaZnOS system. The TTL of the state (0/+) is E_V+0.51 eV above the VBM (i.e. E_V for VBM), and the TTL of the state (+/2+) is E_V-0.30 eV below the VBM. From the formation energy versus the E_F, the Cu_{Ca}^{0} is the relatively stable doping state within most range of E_F of the gap above the E_V+0.51 eV. The neutral doping state of Cu_{Ca} in CaZnOS has a formation energy is 5.20 eV and 1.85 eV under chemical potential of S-rich and Zn-rich limits respectively. The formation energy of Cu_{Ca}^{+} is estimated as 4.69 eV and 1.34 eV respective under S- and Zn- rich limits. As discussed above, the relative position of TTL (0/+) in the band gap for Cu_{Ca} is obtained to be the position near the VB edge, in a good agreement with energy diagram by Xu et al [5]. However, the formation energy of Cu_{Ca} is obviously higher than Cu_{Zn} in CaZnOS with more than 2 eV in energetic magnitude.

Mn_{Zn} doping

We turn to the case of Mn doping on substituting the Zn site from CaZnOS, which is a potential application for red-luminescence with emission wavelength of ~610 nm from experiment [32, 33].

From the partial density of states targeted on Mn doping site, for the neutral satte (Mn_{Zn}^{0}), we found there are a few extra deep donor levels from their single-particle level in the PDOS (Figure 4 (a)). Their localized electronic levels are staying at E_V+0.096 eV, E_V+0.263 eV, and E_V+0.358 eV above the VBM (E_V denotes the VBM). While the localized hole levels are contributed by the Mn 3d-fine levels and in spin-down configuration, with E_V+4.578 eV, E_V+4.604 eV, E_V+4.679 eV, E_V+4.726 eV, E_V+4.906 eV, and E_V+4.977 eV respectively, buried into the conduction band region of host CaZnOS. The energy interval between the lowest hole level and highest electronic level is 4.578 eV, which is far beyond the emission photon energy (~2.03 eV) of experimental reported luminescence (~610 nm)[32, 33]. Thus, we deduced that the emission photon energy may not be sourced from the direct de-excitation from the excited Mn level to ground state level correspondingly.

For the Mn_{Zn}^{+} doping state, the localized electronic levels are staying at E_V+0.071 eV, E_V+0.154 eV, and E_V+0.193 eV above the VBM, while the localized hole levels are distributed in two regions near the band gap, one part is at VB edge with spin-up as a shallow hole level, the other is spin-down sitting at CB edge consisting fine levels of localized hole states as nearly a deep acceptor bands (Figure 4 (a)). The spin-up shallow hole level is E_V+0.460 eV higher than the VBM in the gap. The spin-down deep hole bands are distributed into five fine levels with energetic intervals of about 0.05 eV~0.2 eV. They are E_V+4.224 eV, E_V+4.313 eV, E_V+4.375 eV, E_V+4.558 eV, and E_V+4.661 eV respectively resident in the conduction band, in a uniform trend align with the case of Mn_{Zn}^{0}. Similarly, the minimum energy interval between spin-up electronic and spin-down hole level is 4.031 eV, and slightly wider than the Mn_{Zn}^{0} state. The minimum interval between spin-up and down hole level is 3.764 eV, close to the magnitude of the optical fundamental band gap of host CaZnOS.

For the Mn_{Zn}^{2+} doping in CaZnOS (Figure 4 (a)), there are two localized electronic levels are staying at E_V+0.032 eV and E_V+0.146 eV above the VBM acting as deep donor state, while the localized hole levels are showing similar behavior to the case of Mn_{Zn}^{+}. There are two spin-up shallow hole levels are staying at E_V+0.322 eV and E_V+0.419 eV above the VBM in the gap. For the spin-down deep hole levels, they present as fine-levels with very small energetic intervals below the conduction band minimum (CBM). Moreover, such fine-levels consist a hole band that overlap with CB edge, with part of in the delocalized CB region and the rest fall into the band gap area below the CBM. The relative positions of such fine-levels are given as E_V+3.668 eV, E_V+3.835 eV, E_V+3.897 eV, E_V+4.031 eV, and E_V+4.121 eV respectively. The energy interval between the above higher spin-up hole level and the lowest spin-down hole level are 3.249 eV, while 3.522 eV for the interval between the highest electronic level and the lowest spin-down hole level.

From the above analysis, the native luminescence for electrons de-excitation for Mn in three different charge state are not the direct contributing source of ~610 nm luminescence.

Figure 4 (b) shows the orbitals of the localized electrons and holes levels induced by Mn_{Zn} in CaZnOS. The neutral doping state shows the electronic levels have an evident p-d orbital coupling effect between three Mn_{Zn}-S and Mn_{Zn}-O bonds. The Mn is showing a $3d_z^2$ and orbital feature, and also a linear combination of $3d_{xy}$ and $3d_{xz}$ components for the third electronic state next to the VBM. The hole fine-levels given by the Mn_{Zn} in neutral state are showing isolated 3d orbitals with different components or combinations, with energy band width of 0.393 eV. In Mn_{Zn}^{+} state, one of the hole level turns down the level where is near the electronic state. Due to the electron-hole Coulomb attractive effect, the orbital of such state still keeps the p-d coupling feature localizing between Mn_{Zn}-S and Mn_{Zn}-O bonds. In the Mn_{Zn}^{2+} doping state, the hole levels near the VBM are showing similar p-d coupling effect around the local structure of [3S-Mn_{Zn}-O].

The formation energy of Mn_{Zn} at 0, +1, and +2 charge state is indicated in Figure 4 (c). The trend in physical chemistry shows that the neutral formation energy is more energetic favorable compared to the Mn_{Zn} doping. Similar effect has also been found from our previous work in CaS system with Eu and Dy doping [34]. It also indicates a positive-U_{eff} for the Mn_{Zn} in CaZnOS experiencing a charge transition from the defect reaction process: $2Mn_{Zn}^{+} \rightarrow Mn_{Zn}^{0} + Mn_{Zn}^{2+}$, with value of +0.11 eV. This means the concentration of Mn doping sites in singly positive charge state may be higher than the one at Mn_{Zn}^{0} or Mn_{Zn}^{2+} state. The TTL of the (0/+) state is E_V+0.34 eV above the VBM and the TTL of the state (+/2+) is E_V+0.23 eV above the VBM. From the E_F dependent formation energy, the Mn_{Zn}^{0} is stable in most area of the band gap from E_V+0.34 to E_C=3.90 eV (CBM). The neutral formation energy is -0.33 eV and -2.31 eV for Mn doping at the Zn site in CaZnOS, under chemical potential of S-rich and Zn-rich limits respectively. The reason of the negative formation energy is analyzed in two different ways. One, it shows a physical chemistry trend that the Mn_{Zn} doping is energetic favorable as the Mn has very similar ionic radius to the one of Zn in CaZnOS. Another reason is the formation energy versus the E_F calculation by DFT is performed under the 0 K conditions. If we extrapolate the related chemical potential terms in Gibbs free energy $\Delta G = \mu_0 + \mu(p, T)$ for the formation of Mn_{Zn}, we may obtain the positive formation energy under ambient condition (300 K, RT) or at even higher temperature during the synthesis process. Therefore, such formation energy calculation can be a good reference when compared to other doping species at the Zn site such as Cu_{Zn} above, i.e., Mn_{Zn} is more dopable than Cu_{Zn}.

Mn_{Ca} doping

We turn to look at the case that Mn substitutes the Ca site in the CaZnOS. The PDOSs of the Mn_{Ca} are shown in Figure 5 (a) with 0, +1, and +2 charge states. For the Mn_{Ca}^{0} doping state, there are two localized electronic levels with E_V+0.162 eV and E_V+0.206 eV above the VBM in spin-up direction. The localized holes are similarly distributed at the fine-levels inside the CB region, which are E_V+4.592 eV, E_V+4.917 eV, E_V+5.115 eV, E_V+5.181 eV, and E_V+5.206 eV respectively with all spin-down configuration. The minimum energy interval between the electron and hole levels are 4.386 eV, which has been already exceeded the optical fundamental band gap limit (3.90 eV).

For the singly positive state (Mn_{Ca}^{+}), there also shows two spin-up electronic levels localized above the VBM with E_V+0.153 eV and E_V+0.213 eV. One of the hole state shifted into the gap with E_V+0.522 eV above the VBM with spin-up. The other holes are all spin-down and

distributed at the unoccupied fine-levels starting from the CB edge to the regions inside the CB, which are E_V+3.891 eV, E_V+4.044 eV, E_V+4.197 eV, E_V+4.347 eV, and E_V+4.481 eV respectively. Similarly, it is relative large for the minimum energy interval between the electron and hole levels, which are 3.678 eV. While for the interval between spin-up and spin-down hole levels, it is 3.582 eV.

For the Mn_{Ca}^{2+}, there are no localized electronic states induced by Mn_{Ca} at charge state +2. All of the localized states are unoccupied and acting as hole levels in two parts in the gap. One part is spin-up with E_V+0.302 eV and E_V+0.400 eV above the VBM in the gap. The other part is spin-down and almost evenly distributed as fine-levels for holes or excited electrons induced at Mn_{Ca}^{2+} site. This part with fine-levels are actually different from the other two state, Mn_{Ca}^{0} and Mn_{Ca}^{+}, since the levels are all well below the CB edge in the optical fundamental band gap region. The levels are E_V+3.243 eV, E_V+3.284 eV, E_V+3.328 eV, E_V+3.459 eV, and E_V+3.465 eV respectively. The minimum energetic interval between spin-up and spin-down hole levels is 2.843 eV.

The localized orbitals of the corresponding electronic and hole levels in the gap are shown in Figure 5 (b). For the neutral doping state (Mn_{Ca}^{0}), the orbitals of electronic levels near the VB are showing an interaction among 3d of Mn, 2p of O and 3p of S sites. The $3d_{xy}$ type orbital component is presented on the Mn site for larger overlapping with the adjacent p orbitals of nearby S and O sites. For the deep acceptor levels as seen inside the CB, all of the orbitals are isolated on the Mn sites with either single or combined d orbital combinations. For the Mn_{Ca}^{+} state, the orbital distribution for the electronic state seems to be weaker than the one in neutral state (Mn_{Ca}^{0}). It indicates us that the ionized electrons at the excited state are not purely sourced from the Mn doping site, in fact, it may be provided from the unity of charge density distributed around the local structural motif of [3S-Mn-3O]. One of the hole is staying near the VB with a strong p-d coupling effect near the S-Mn-O local area. The other five localized orbitals are the five representative fine-levels of holes given by the Mn at the excited state, where are locating at the position overlapped with CB edge. For the Mn_{Ca}^{2+}, all of the localized orbitals are representing the hole levels as there are no electrons localized. These include the hole levels sitting near the VBM with spin-up and hole fine-levels that well below the CBM, given by Mn^{2+}.

Figure 5 (c) shows our DFT calculated formation energy at three charge states, 0, +1, and +2 for Mn_{Ca} in CaZnOS. It seems to be a doping center with negative-U_{eff}, with value of -0.07 eV. This shows the defect reaction process for $2Mn_{Ca}^{+} \rightarrow Mn_{Ca}^{0} + Mn_{Ca}^{2+}$ could be easily affected by external conditions, and is able to be either exothermal or endothermal process, since the $|U_{eff}|$ is too small. The neutral formation energy of the Mn_{Ca} is 0.49 eV and -2.86 eV under the chemical potential limits of S-rich and Zn-rich at 0 K. Recall the Mn_{Zn}^{0} at S-rich limit, its formation energy is found to be -0.33 eV estimated at 0 K by DFT. This evident energetic contrast accordingly implies that the Mn_{Zn} is found to be more easily doped than Mn_{Ca} does. The TTL of the state (0/2+) on Mn_{Ca} site is 0.28 eV above the VBM showing a deep donor like dopant in the CaZnOS system, as similar range as the Mn_{Zn} provided.

Energy levels in luminescence

Dopants and photo-generated native point defects

Before the discussion on the luminescence mechanism, we need to look at the doping limit for the CaZnOS determined by the native point defect levels. As shown from our previous work on CaS system, we illustrate that the dopable range is actually determined by the lowest formation energy defects, in which the external doping would not cause the spontaneous formation of opposite charged defects in the host [34]. Here, as indicated in Figure 6 (a) and (b), we combined the all discussed native point defects at different charge states from the previous work [30], with currently considered Cu_{Zn}, Cu_{Ca}, Mn_{Zn} and Mn_{Ca} at the charges of 0, +1, and +2, under the chemical potential limits of S- and Zn-rich.

From Figure 6 (a), in S-rich limit, the dopable range represented by E_F position is from E_V+1.015 eV to E_V+1.422 eV as shown in orange shaded area. This arises because the Zn_i^{2+} and V_{Zn}^{2-} in the band gap area through the most region of E_F are the lowest formation energy defects. This behavior is different from the finding in the previous studied CaS system [34], indicating the CaZnOS are totally different from CaS. Therefore there have been shown some subtle interplays between the Mn_{Zn} and V_{Zn}^{2-} or Zn_i^{2+}, as the Zn site is the most easy substitution site for Mn to be doped in CaZnOS. Moreover, the Mn_{Zn} shows the lowest formation energy behavior near the dopable range, but the V_{Zn}^{2-} and Zn_i^{2+} surpass the Mn_{Zn} to be the lowest energy defects in the rest of E_F range within the band gap region. Therefore, Mn_{Zn} doping in the system would have a large possibility of causing the formation of V_{Zn} or Zn_i nearby. While the detail charge states may varies from the as-discussed above, but the physical chemistry trend in Gibbs free energy model will remained rigidly.

For the Cu doping, they are costing higher energy than Mn does. Besides, the Cu_{Zn} is obviously lower than the Cu_{Ca} through whole E_F range of the band gap. Meanwhile, below the TTL of (0/2+), the formation energy diagram of V_{ZnO}^{2+} almost merges with the Cu_{Zn}^{2+}. This means below the TTL of (0/2+) for Cu_{Zn}, the V_{ZnO}^{2+} and Cu_{Zn}^{2+} are energetically un-separated, i.e., the V_{ZnO}^{2+} and Cu_{Zn}^{2+} are energetically equivalent and are formed in CaZnOS with equivalent possibility. Accordingly, the V_{ZnO}^{2+} may act an intermediate level for transfer the holes from Cu_{Zn}^{2+} so as to transfer/forward the original activator (sensitizer) site (Cu_{Zn}^{2+}) to a new designated activator site (V_{ZnO}^{2+}). We have gained related experience through our previous work in cubic Cu_2O where the deep hole trap levels are found through two types of intrinsic defects [52]. Moreover, we also found that the V_{CaZnOS}^{0} shows relatively higher than the Cu_{Zn}^{0} formation energy level for the 0 and +2 charge state, but turns to be lower starting from E_V+2.0 eV at the charge state of -2. These clues promoted us to further investigate through the discussion on the single-particle levels of dopants and native point defects in CaZnOS, in a clearer picture.

Figure 6 (b) shows the native point defects formed under Zn-rich limits. The dopable range gets narrower than the case found in Figure 5 (a). Differently, in CaS system, the dopable ranges in Ca- and S-rich limits have equivalent energy widths in E_F within band gap area. However, in CaZnOS, the chemical potential limits are supposed to consider four different cases coming with a difficulty in calculations. With consideration of experiments[67], the S- and Zn-rich are mostly covering the experimental synthesis conditions, of course, with some extent of imperfections. This would not affect us to discuss the doping formation energy levels of Cu and Mn in CaZnOS.

We found the Cu_{Zn} are obviously moving above the V_{ZnO} formation diagram. Both the Mn_{Zn} and Mn_{Ca} are well below the all native point defects energy levels, and the Mn_{Ca} turns to be the lowest formation energy doping under the Zn-rich potential limit. Therefore, even under the metallic element rich potential limits for synthesis conditions of CaZnOS system, the formation of Cu and Mn substitution doping will obvious cause formation of some native point defects from the host lattice. This will provide a solid reference for our further investigation on the mechanism of luminescence found in Cu-doped [5] and Mn-doped system respectively[32, 33].

Another highlight is worth mentioning is that, though the photo-irradiation is usually takes the bounded electrons from the top of VB to the CB for the host lattice, it is also an external source of energy transferred into the host resulting into a generation of the native point defects. We may call it as photo-generated native point defects for understanding the subtle interplaying relationship between native defects levels and photo-sentitizer typed dopants. In addition, as we know, experimental photo-excitations wavelengths are reported in the range from 280 nm [33] to 304 nm [43], which is about the range from 4.08 eV to 4.43 eV in photon energy. The above high energy photo-irradiation has indeed reached the energy levels that can generate most of the native point defects from the host lattice, as shown from either Figure 6 (a) or (b).

Inter-transitions between single-particle levels

a. Luminescence induced by Cu substitution doping

Figure 6 (a) shows that, the doping sites such as Cu_{Zn} and Cu_{Ca} generally have higher energy than the most native point defects, and Cu_{Ca} has higher cost energy to form than the Cu_{Zn}. This energy difference is about 2.2 eV high. Therefore, it is reasonable to consider the electronic properties contributed by Cu_{Zn} only.

We combined the single particle levels of native point defects with Cu_{Zn} and Cu_{Ca} for the charge states of 0, +1, and +2, as indicated in Figure 7 (a). As discussed from the above section, the Cu_{Zn} doping produced the deep hole trap levels near the mid-gap area with 2.57 eV and 2.67 eV below the CBM for Cu_{Zn}^{+} and Cu_{Zn}^{2+} respectively. The Cu_{Ca}^{0} and Cu_{Ca}^{2+} contribute the electronic de-excitation paths with energy intervals of 2.64 eV and 2.58 eV respectively. However, the formation energy of Cu_{Ca}^{0} is too high throughout the optical band gap area, even for the Cu_{Ca}^{2+} within the VB area under the S-rich limit. Basically, the optical transitions between s and d orbitals are parity forbidden by selection-rule. However, as seen from the PDOS analysis, the CBM consists of a partially hybridized s and p orbitals, this will increase the possibility of the optical transition or to higher optical oscillator strength, as p→d optical transition is allowed.

As illustrated in the Figure 7 (a), the external energy excitation approaches in way of 980 nm near-infra-red (NIR), UV irradiation, and mechano-stimulus, by the vertical dark brown, black, and green arrows respectively. Especially for the green vertical line, different scale of mechano-stimulus has been shown and can effectively pump-up electrons gradually from the localized electronic trap levels to a higher state near CBM or in the CB region. With initially UV-irradiation (365 nm, i.e. 3.40 eV) by experiments [5], the electrons at the Cu_{Zn}^{0} doping site are

easily excited into a higher state and ionized themselves into the CB range by a small energetic threshold.

We then look at the role of Cu_{Zn}^{+}. As we discussed above, the Cu_{Zn} is a negative-U_{eff} center that denotes Cu_{Zn}^{+} exists in the host lattice (CaZnOS) in a low concentration or with a short life-time. This doping state has also acted as a luminescence activator center with emitting 2.57 eV photons or 482 nm in wavelength. As the life-time for electron occupation on this level is short, it will be further transfer to another state for luminescence, which is the V_{ZnO}^{2+} since they are energetically equivalent as discussed in previous section (Figure 6 (a)). This has further confirmed, slightly modified, and enriched the proposed mechanism by experiment of Xu et al [5], and the data are shown in agreement with experimental report [5].

A trend is thus following as (1) $Cu_{Zn}^{0} \rightarrow Cu_{Zn}^{2+}$ by external high-energy UV irradiation; (2) $Cu_{Zn}^{2+} \rightarrow Cu_{Zn}^{+}$ by capture the electrons de-excited from CBM at Cu_{Zn}^{2+} site; (3) $2Cu_{Zn}^{+} \rightarrow Cu_{Zn}^{0} + Cu_{Zn}^{2+}$ by negative-U_{eff} effect; and (4) $h(Cu_{Zn}^{2+}) \rightarrow h(V_{ZnO}^{2+})$ by hole drifting effect as the higher localized hole levels the more stability of hole reaches, also the formation energy diagram of Cu_{Zn}^{2+} and V_{ZnO}^{2+} are merged as energetically equivalent. By process (2), the luminescence wavelength is shifted from 464 nm (2.67 eV) to 482 nm (2.57 eV) in a short time, in consistent with experimental reported red-shift from 472 nm (2.63 eV) to 483 nm (2.57 eV) within time-duration of 1 min. Due to increased amount of Cu_{Zn}^{+} given by process (2), negative-U_{eff} effect will drive the process (3) in trend of physical chemistry and the electrons are transferred by non-radiative process, this may takes 5 min in transition as indicated by experiment of Xu et al [5]. The process (4) will further by driving force of lower Gibbs free energy represented by formation energy calculation. The Cu_{Zn}^{2+} and V_{ZnO}^{2+} are energetically equivalent, and a significant hole-drifting takes effect due to lower energy level for holes to transport towards (shown by red curved arrow in Figure 7 (a)). After process (4), the photo-sensitizer center is transferred to the V_{ZnO}^{2+} site and the emission peak of phosphor luminescence is stabilized at the 496 nm (2.50 eV), as 20 min long as shown in experiment [5].

Another interesting experimental observation is necessary to be considered in our calculation is the mechanical quenching. Xu et al observed both reversible and un-reversible mechanical quenching effects (R-MQ and UR-MQ) during the phosphor luminescence of 472 nm for Cu-doped CaZnOS [5].

We elucidate the small energetic scaled mechano-stimulated electron-hole recombination in Figure 7 (b). This is a simplified diagram to draw-out the paths how electrons recombine with holes non-radiatively for quenching the photon-emission at the activator sites. This arises because of two factors, one is the Cu_{Zn} formation energy is higher cost than most of native point defects. The existence of Cu_{Zn} usually comes with some native point defects levels as shown in Figure 6 (a). Thus, it is necessary to combine the contributions of electronic levels given by the native point defect levels with the localized hole level of Cu_{Zn}^{2+}, for our consideration.

As summarized from our previous work [30], for instance, V_{Zn}^{0}, V_{Zn}^{-}, V_{Zn}^{2-}, S_i^{0}, and O_i^{0} induce localized electronic levels above the VBM and below the localized hole levels of Cu_{Zn}^{2+}. The V_{ZnO}^{0}, V_{ZnO}^{-} V_O^{0}, V_{CaZnOS}^{-}, V_{CaZnOS}^{2-}, a-Fr_O^{0}, and a-Fr_O^{+} has crossover range for formation energies and can provide electronic levels slightly higher than the hole level of Cu_{Zn}^{2+}. The O_i^{2-},

a-Fr_O^-, and a-Fr_O^{2-} can provide both higher and lower than the hole level of Cu_{Zn}^{2+}. Xu et al has also proposed that the V_{Zn} is one of the defects responsible to the MQ effect [5], and it acts as deep non-radiative center. From our calculations, we further confirm their analysis, but also classified the different contributions by V_{Zn} within different charge states in detail. The V_{Zn} in all charge states (0, +1, and +2) are found to be the R-MQ center.

It is also interesting to note that, the UR-MQ centers contributed by the native point defects above are also responsible to enhance the phosphorescence intensity when external mechano-stimuls is loaded on the sample after 12 hr long [5]. This arises because, such a long enough time-duration past indicates the Cu_{Zn}^{2+} all turns back to the Cu_{Zn}^{0} state, or transfer the activator center to the V_{ZnO}^{2+} or V_{CaZnOS}^{2+} sites by process (4) summarized above. With the increase of the loaded mechano-stimuls, the trapped electrons on the filled state are subsequently excited to the higher state near the CBM or at the CB edge. These mechano-excited electrons (as indicated by green arrows) will de-excited back and recombine the holes at the V_{ZnO}^{2+} or V_{CaZnOS}^{2+} sites. The higher load of external mechano-stimulus, the more amount of electrons are promoted to be excited level near the CB edge. Therefore, the phosphor luminescence intensity has been increased accordingly.

Another thing is the consideration on the defects with very low formation energy. Especially for the O_i, as shown in Figure 6 (a) and discussion we provide previously, it has very low formation energy rather close to the zero formation energy level. Therefore, it is almost a freely mobile state in the S-rich chemical potential limits. According to the electronic levels that localized near the VBM or deep in the gap by O_i^0 and O_i^{2-} respectively, such type of defect (O_i) is the phosphor luminescence "killer" by mechanical-stimulus. As the ionic radius of O is relatively small, the sample powder of as-synthesized CaZnOS exposure in the air under the ambient conditions are very easily absorbing the O_2 molecules or $O_2^{\delta-}$ ($0<\delta<2$) and they are dissolved into the lattice with forms of O atoms or ions respectively. This process will generate large O_i throughout the host CaZnOS lattice, playing as mobile MQ center carrying opposite charges. Moreover, it has formation energy lower than the Cu_{Zn}, and needs to be external mechano-stimulus to promote its level to be energetically equivalent to the Cu_{Zn} state.

We schematically classified and summarized the R-MQ and UR-MQ energetic regions for the phosphor luminescence by Cu_{Zn}^{2+} in CaZnOS. As indicated in Figure 7 (b), the solid curved violet arrow denotes the R-MQ process that, electrons occupying the localized levels below the E_V+1.2 eV of Cu_{Zn}^{2+} in the band gap are capable to be excited to recombine the holes staying on such level, while it will turn backward to the original electronic levels as the lower electronic level the more stability of electrons reaches in physical trend. Conversely, the dashed curved violet arrow denotes the UR-MQ process that, the electrons will be activated with a small energetic threshold to drop on the hole state where is 1.2 eV above the VBM non-radiatively. These electrons will hardly come back as the energy levels are higher than the level of E_V+1.2 eV, and the higher electronic level the higher backward energy barrier for electrons.

b. Luminescence induced by Mn substitution doping

We turn to look at the case of Mn doping in CaZnOS. The Mn^{2+} activated CaZnOS has been firstly systematically studied by Duan and Hintzen [43], whose experiment show that a phosphor

emission ranged from 550 nm (2.25 eV in photon energy) to 700 nm (1.77 eV in photon energy) and can be assigned into the transition between $4T_1(^4G) \rightarrow 6A_1(^6S)$. More recent study shows an extensive detailed characterization of that phosphor luminescence and discovered a red-shift of the luminescence, and amount of luminescence related properties are dependent on the Mn^{2+} doping concentrations [32, 33].

Recall some details from Figure 6 that, the energy difference between Zn and Ca substituted Mn doping is about 0.82 eV, with Mn_{Zn} forms 0.33 eV below the zero formation energy and only 0.49 eV above the zero energy level for Mn_{Ca}. Therefore, they are both relatively easy to be doped in CaZnOS, while Mn_{Zn} exists in a slightly higher concentration. On the other hand, this can be understood as the scenario that, in the process of Mn-doping concentration dependent experiment, the Mn will firstly occupy the Zn site and then the Ca site with the dosage of Mn doping gradually increased. Therefore, it shows a trend with gradually increased amount of Mn doping that, the Mn doping from low to high concentration is actually a process from the substitution of Zn- (Mn_{Zn}) to the Ca-sites (Mn_{Ca}).

Moreover in Figure 7 (c), we have shown that the Mn doped CaZnOS contains the 3d fine-levels are staying above the CB, at the CB edge, and below the CB or overlapped, for the charge states of 0, +1, and +2 respectively. This is also consistent for both Mn_{Zn} and Mn_{Ca}. The energy band width for the 3d fine-levels near the CB shows about 0.5 eV in average for Mn_{Zn} with a small difference, while 0.3 eV~0.7 eV for the width given by the Mn_{Ca} (actually, 0.3 eV for charge state q=0, 0.5 eV for q=+1, and 0.7 eV for q=+2 respectively). Two experiments conducted at different time-stage both showed the absorption band width from the $4T_1(^4G)$ to $4T_2(^4D)$ in corresponding energy of 0.67 eV in the maximum[33, 43]. This is given by the energy difference from the absorption peaks of $4T_1(^4G)$ (~510 nm, i.e. 2.43 eV) and $4T_2(^4D)$ (~400 nm, i.e. 3.10 eV), respectively [33, 43]. Our calculated band width shows a good agreement with the experimental observations, and denotes the possible coexistence of Mn_{Zn} and Mn_{Ca}.

Figure 7 (c) shows the paths of luminescence by electron-hole recombination. The dark brown, black, and green arrow vertically denotes the different manner of external excitations on electrons, such as 980 nm near-infra-red (NIR), 200 nm~300 nm UV irradiation, and mechano/tribo-stimulus in local lattice piezo-electrical energy, respectively. Meanwhile, the opposite charged holes are also correspondingly being excited by the same manner and locate at the localized hole states in the optical band gap or near the VB/CB edge. This process is called spatial charge separation by native point defects, as illustrated in our previous work, Fig 1 of ref[30], and the external energy was then subsequently harvested at such localized levels. The excited electrons which is denoted as "**e***" in Figure 7 (c) will fall back the lower energy levels to recombine the excited holes and release energies in way of photon emissions at the specific levels.

We further noted that, the Mn_{Zn} doping sites distributing among the host lattice are actually seen as the Mn occupies the intrinsic V_{Zn} sites in CaZnOS that are natively formed during the synthesis process. Thus, the single-particle levels between them are correlated from some extent. The localized hole state at E_V+1.7 eV is given by the V_{Zn}^- calculated previously [30] and also shown in Figure 7 (c), while such state is not relatively stable compared to Mn_{Zn} according to the formation energy calculation under the S-rich (or Zn-poor for Zn deficit, i.e. for V_{Zn}) limit. It

will capture an additional electron to form V_{Zn}^{2-}, and hence stay below the Mn_{Zn}^{0} formation energy diagram (Figure 6 (a)) reaching to an even more stable state than Mn_{Zn} through the band gap area. The trapped de-excited electron will consequently transferred back to the levels that close to the VB edge or inside of VB region, which is originally excited from the VB or levels near the VB edge.

From the Figure 7 (c), the higher shallow localized hole level induced by Mn_{Zn}^{2+} is occupying above the VBM with the E_V+0.42 eV. Based on this level, we also found another path is shown as phosphor luminescence from the localized electronic level of V_{ZnO}^{-} to the E_V+0.42 eV, which is representing the electron moving towards to lower energy where the hole is staying at. From Figure 6 (a), the formation energy of V_{ZnO}^{-} versus the E_F within the band gap is not relative stable compared to the Mn_{Zn}^{0} and Mn_{Zn}^{2+}, thus the electrons that are occupying at the V_{ZnO}^{-} sites will transfer towards to the localized shallow hole levels provided by Mn_{Zn}^{2+} in the band gap, and release the energy in forms of photon emissions. The photon energy is about 2.1 eV consistent with experimental observed emission peak positions of 2.02 eV (614 nm). Thus, there are two proposed paths for Mn_{Zn}^{2+} induced phosphor luminescence. One is from $4T_1(^4G)$ of Mn_{Zn}^{2+} to the V_{Zn}^{-}, while the other is from V_{ZnO}^{-} to the $6A_1(^6S)$ of Mn_{Zn}^{2+}.

Experimentally also reported another evident phosphor luminescence with emission peak at about 530 nm (i.e. 2.34 eV in photon energy) but in a lower intensity[33]. For the peak levels, we found from the single-particle levels calculations results reported previously, the V_{ZnO}^{2+} is a suitable site that carries the excited electrons to attract them within a short life-time passing through the localized hole levels to recombine the holes occupying at the lower level (EV+1.35 eV). The V_{CaZnOS} shows similar behavior discussed previously, but in an even higher cost energy to transport the electrons between Mn_{Zn}^{2+} and V_{CaZnOS}^{2+} under S-rich chemical potentials. Therefore, the V_{ZnO}^{2+} is the only suitable native point defect levels for collaborative phosphor luminescence to contribute the experimentally reported 530 nm emission. Our calculated energy interval for such optical inter-level transition is 2.32 eV (i.e. 534 nm in wavelength), in a good consistency to experimental observation[33]. Due to the relatively high cost energy of V_{ZnO}^{2+} compared to Mn_{Zn}^{2+} in CaZnOS, the charge carrier recombination activity between these two sites comes to be a minority. The optical emission intensity thus gets lowered than the dominant 614 nm emission [32, 33, 43].

Figure 7 (c) also shows that the hole level given by V_{Ca}^{0} from the host lattice seems also to be a suitable level that merges with $4T_1(^4G)$ of Mn^{2+} to form a combined activator site. Under the S-rich limit, this is also confirmed from the formation energy diagram that, above the TTL of state (2-/-) for V_{Zn}, the energy diagram of V_{Ca}^{2-} and V_{Zn}^{2-} are almost merged and acting as energetically equivalent sites for such combined activator center of Mn^{2+} doped phosphor luminescence in CaZnOS. While for the potential limit of Zn-rich, the V_{Ca}^{2-} almost overlaps with the energy diagram of V_{ZnO}^{2-}. We thus deduced that, the V_{Ca}, V_{Zn} and V_O sites are mutually interacting with each other under an unknown mechanism, which will be explored in the future work.

Now for the Mn_{Ca}^{2+} state, the transition width between $4T_1(^4G)\rightarrow 6A_1(^6S)$ is found to be 2.84 eV in CaZnOS system. The optical transition between these two states is too wide to match the experimental observed 614 nm phosphorescence. Formation energy calculations show that the

Schottky type V_{CaZnOS} defect can be formed below the formation energy of Mn_{Ca} doping within the band gap area shown in Figure 6 (a), and the related energy diagram is also close to the V_{Ca} even under the metallic rich potential limit (Figure 6 (b)). Based on our previous single-particle level calculations on native point defects, the V_{CaZnOS} has two localized hole states that within the band gap area, with one is about 0.2 eV below the CBM, and the other is E_V+1.23 eV above the VBM [30]. From the TDOS calculation on Mn_{Ca}^{2+}, the lowest excited state $4T_1(^4G)$ is sitting below the CBM which is E_V+3.24 eV (E_V for VBM), therefore, the optical inter-level transitions between this energy interval will release the energy in form of photons of about 2.01 eV (or 617 nm), in a close agreement with experimental observed phosphorescence with peak centered at 614 nm [32, 33, 43].

c. Concentration quenching effect by Mn doping

Original experiment done by Hintzen et al has shown that the Mn^{2+} in CaZnOS activated an efficient red luminescence with single peak fixed at 614 nm regardless of the doping concentration variation effect[43]. Further detailed work presented a red-shift of the peak with movement of 12 nm, representing a photon energy difference of 0.04 eV[33]. As our analysis above, this arises because the localized hole levels that accommodates the de-excited electrons are drifting from V_{Zn}^- to the V_{Ca}^0, through a spatial charge transportation or tunneling effect if these two defects are stay within a close distance. Also, according to Figure 7 (c), our calculated single-particle levels show the energetic difference of these two localized hole levels is 0.05 eV, which is from 620 nm to 635 nm (red-shift of 15 nm), in a good agreement with experiment within acceptable error magnitude. Why this happens? This arises because, the holes are drifting from the original V_{Ca}^0 site onto the V_{Zn}^- site, and Figure 6 (a) also confirms that the V_{Zn}^- has lower energy than V_{Ca}^0 near the VBM. The free holes will drift from the original V_{Ca} to the V_{Zn} site and photon energy emission (via the inter-level transitions) is red-shifted to a lower energy.

Another interesting effect reported by experiment is summarized into the concentration quenching effect. First of all, the optical band gap decreased with increased doping amount of Mn, due to red-shift of photo-absorption edge. From the above analysis together with Figure 6 (c), we see that the $4T_1(^4G)$ level were all below the CBM for the Mn_{Zn}^{2+} and Mn_{Ca}^{2+} doping state, while the one in Mn_{Ca}^{2+} presents to be lower (E_V+3.243 eV) than the Mn_{Zn}^{2+} (E_V+3.668 eV). We used a relative position fraction to represent them as, the $4T_1(^4G)$ level of Mn_{Zn}^{2+} is occupying the 6% of the E_g (E_g denotes the band gap of host, 3.90 eV by our calculation) below the CBM, while 17% of E_g for Mn_{Ca}^{2+}. Compared with experiment, it is found that 6% of the E_g for Mn_{Zn}^{2+} while 11% for Mn_{Ca}^{2+} [33], showing a good consistency between our calculations and experimental observations.

As indicated in Figure 8 (a), after the doping, the measured optical band gap by photo-absorption spectra is attributed to the optical vertical transitions of $VB \rightarrow 4T_1(^4G)$ of Mn^{2+}. We have discussed the coexistence of Mn_{Zn} and Mn_{Ca} in previous section as their formation energy difference is only 0.8 eV with zero energy line in the middle. Thus, in a small amount of Mn-doping, the Mn_{Zn} is the dominant doping sites. While with increased Mn-doping concentration, the Mn_{Ca} becomes more and more evident in occupation from the view of thermal equilibrium statistics. Thus, the $4T_1(^4G)$ of Mn_{Ca}^{2+} shifts downwards a deep range away from the CBM,

leading to a decreased optical vertical transition intervals. The measured optical band gap is accordingly decreased with Mn-doping concentration increased from the experiment[33].

The experiment further found the Mn-doping concentration quenching effect, which is a uniformed decreased behavior of brightness/intensity of phosphor luminescence, decay time, and optical band gap width, with increase the Mn-doping concentration. This leads to a question that, if the luminescence ony rely on the optical transitions between d-d levels of $4T_1(^4G)\rightarrow 6A_1(^6S)$, why will it have concentration quenching effect? As discussion on the optical band gap width dependent on Mn doping concentration, we deduced that the quenching effect is also attributed to the occurrence of the Mn_{Ca}, as its neutral formation is also rather low with about 0.3 eV under the S-rich limit. The emission spectra of host lattice observed from photoluminescence (PL), Tribo-ML, Compress-ML, and Ultrasonic-ML and Cathodoluminescence (CL) are all presenting a typical peak doping composition of x=0.003~0.004. This arouses our attention and further interest to carry out a simple approximated model to illustrate the significant role on the co-existence of Mn_{Ca} in the lattice.

First of all, we assume the occupations of V_{Zn} and V_{Ca} are *a* and *b* (*a, b>0*). Considering the thermo-equilibrium statistical effect, the rate of the Mn for occupying the V_{Zn} to form Mn_{Zn} is η_1 and η_2 $(\eta_1, \eta_2 > 0)$ for the case of occupying the V_{Ca} to form Mn_{Ca}. The total doping composition of Mn into the lattice of CaZnOS after thermal equilibrium is shown to be *x* (*x>0*).

For the stage of very low dosage of doping, we approximate that Mn_{Zn} is the dominant doping state and Mn_{Ca} is negligible, which means:

$$\begin{cases} 0 \le \eta_1 x \le a - \eta_1 x \\ 0 \le \eta_2 x << b \\ \eta_2 x \to 0 \end{cases} \quad (2)$$

The intensity represented by I, is yielded within the range as follows:

$$0 \le I =_{\min} \left[(a - \eta_1 x) \eta_1 x \right] \le \frac{a^2}{4} \quad (3)$$

With increased doping concentration of Mn doping, the occupation on V_{Ca} for Mn_{Ca} doping becomes more evident. We consider this is the intermediate range to match the fact that the x is not very large in experiment. The intensity is represented as follows:

$$\begin{cases} a - \eta_1 x \le \eta_1 x \\ 0 \le \eta_2 x \le b - \eta_2 x \\ I = I_{Zn} + I_{Ca} = (a - \eta_1 x)^2 + (b - \eta_2 x) \eta_2 x \end{cases} \quad (4)$$

With this analysis, we plot the relationship between I and x based on the Eq. (3) and Eq. (4), shown in Figure 8 (b) and (c). It is a behavior contains two parabolic-curves with two different opening directions. The peak center is shown as $x = \frac{a}{2\eta_1}$, which is also the turning point between this two different parabolic-curves. Experimental spectra show the uniformed turning-*x* at peak,

it is consistent shown by us that the turning point at $x = \frac{a}{2\eta_1}$ is an intrinsic value that represents the properties of host lattice.

We finally see the formation energy in S-rich limit that, the Mn_{Zn} and Mn_{Ca} are both in an energetically favorable E_F range within the optical band gap. All of the related native point defects form with relatively higher energy than Mn doping. Accordingly, in opinion of formation energy, it further tells us that the related luminescence shall be dominantly considered at the Mn_{Zn} and Mn_{Ca} induced localized levels that within the band gap. This is also following a trend of physical chemistry in chemical potentials for electronic transport. Therefore, previous discussed native photo-activator site such as V_{ZnO} and V_{CaZnOS} with 2.50 eV with energy interval are not the dominant sites of charge carrier recombination for phosphor luminescence, as the excited electrons will firstly come through the levels induced by Mn^{2+} sites and recombine the hole at the levels selected by view of formation energy discussed above.

Conclusion

In summary, motivated by novel discoveries from pioneers and experts[5, 33], we have discussed the transition metal doped CaZnOS with a case study of Cu and Mn doped system. The interplay effect of native point defects is rather significant as an energy relay center among the process of mechanolumienscence. We illustrated that the combinations of native point defects and doping levels yielded two interesting mechanisms respectively in the two doped systems. The energy transfer in luminescence passes via CBM to the Cu-t_{2g} level of Cu-3d orbital localized within the band gap in the Cu-doped system. Its red-shift effect is interpreted by a hole-drifting effect within the band gap. Both reversible and un-reversible mechanical quenching (R-MQ and UR-MQ) effects are attributed to the spatially separated electrons recombine the hole localized on Cu-t_{2g} level within the gap, with levels below or above respectively. Another intriguing mechanism is discussed in Mn doped case, which is native point defects participated collaborated phosphor luminescence. The 3d fine levels of Mn^{2+} doping state is overlap with CBM and the $4T_1(^4G)$ state is below the CBM. Formation energy calculations confirmed the coexistence of Mn_{Zn} and Mn_{Ca} is confirmed but relatively low in Mn_{Ca}. It is a key to explain the Mn doping concentration quenching effect as well as the red-shift of absorption edge. We attached to such finding with simplified approximation and elucidated an intrinsic property of Mn-doped CaZnOS to present a concentration quenching effect.

Acknowledgement

The author BH gratefully acknowledges the support of the Natural Science Foundation of China (NSFC) for the Youth Scientist grant (Grant No.: NSFC 11504309), the initial start-up grant support from the Department General Research Fund (Dept. GRF) from ABCT in the Hong Kong Polytechnic University (PolyU), and the Early Career Scheme (ECS) fund (Grant No.: PolyU 253026/16P) from the Research Grant Council (RGC) in Hong Kong. This work is supported by the high performance supercomputer (ATOM-project) in Dept. of ABCT of PolyU.

Figure 1.

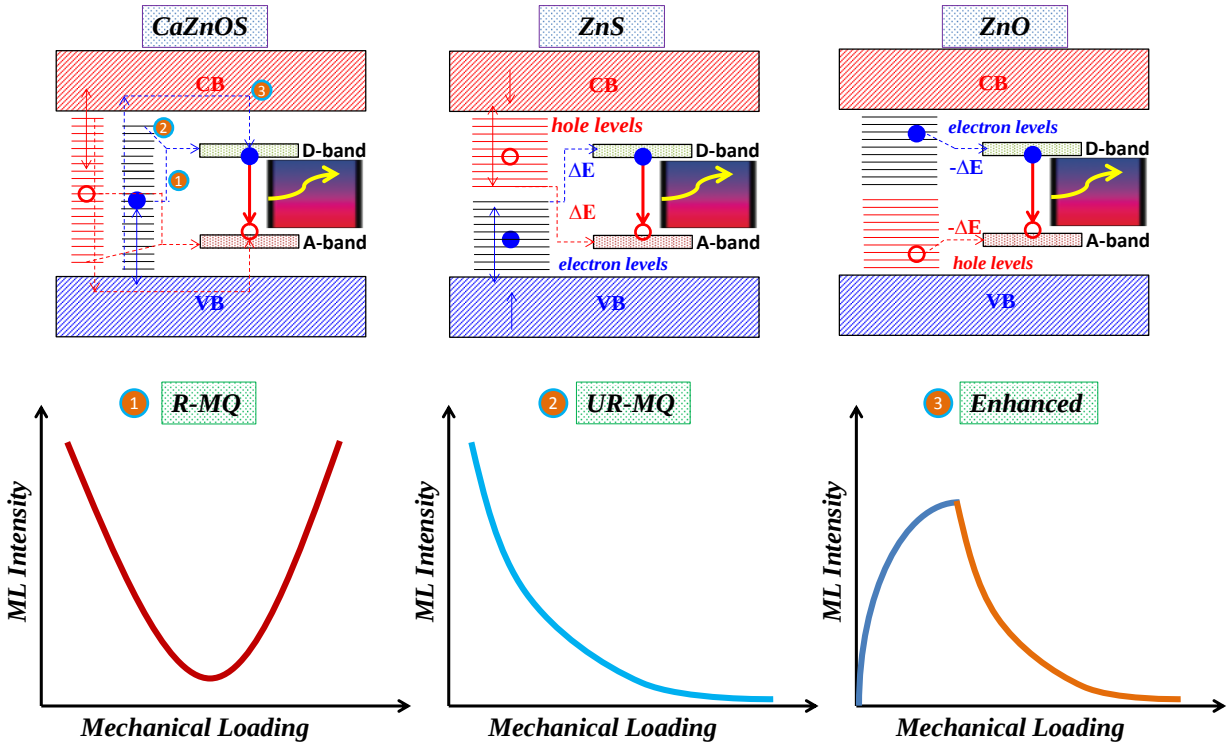

Figure 1. Schematic diagram for reversible and un-reversible mechanical quenching (R-MQ and UR-MQ), as well as Enhanced luminescence by mechanical loading.

Figure 2.

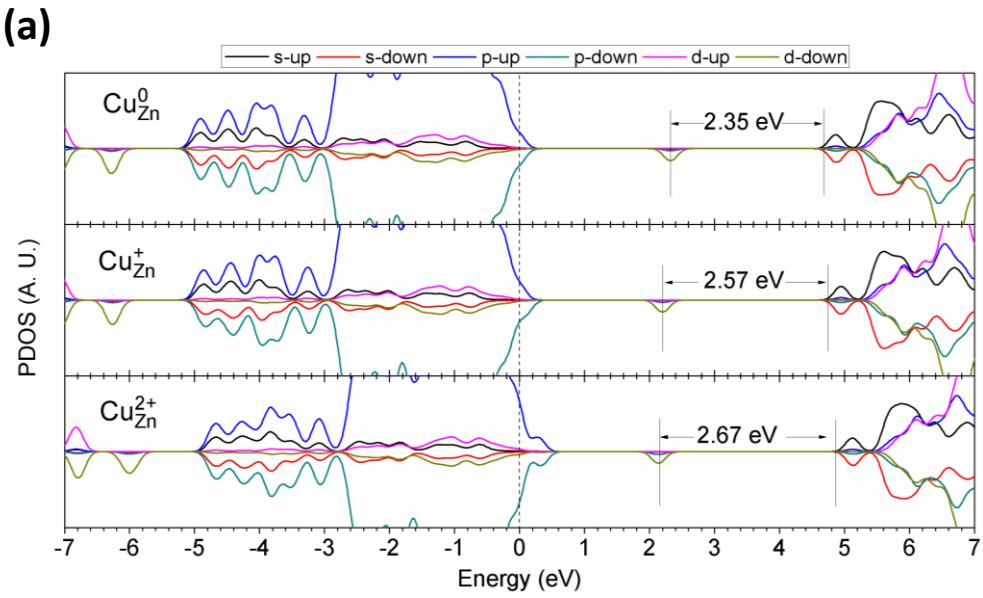
(a)
s-up
s-down
p-up
p-down
d-up
d-down
Cu^{0}_{Zn}
Cu^{+}_{Zn}
Cu^{2+}_{Zn}
2.35 eV
2.57 eV
2.67 eV
PDOS (A. U.)
Energy (eV)
-7
-6
-5
-4
-3
-2
-1
0
1
2
3
4
5
6
7

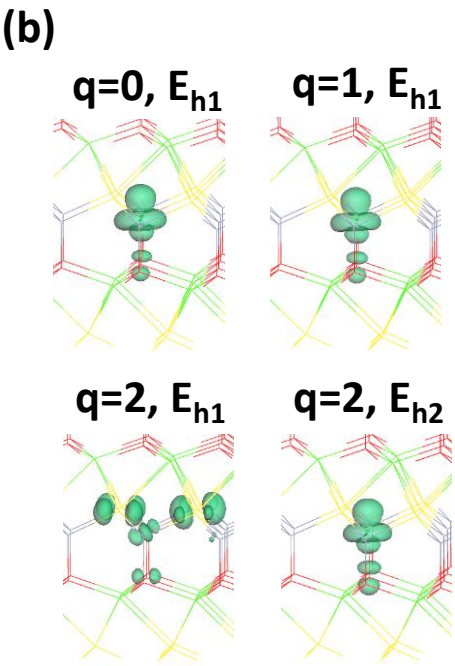
(b)
q=0, E_{h1}
q=1, E_{h1}
q=2, E_{h1}
q=2, E_{h2}

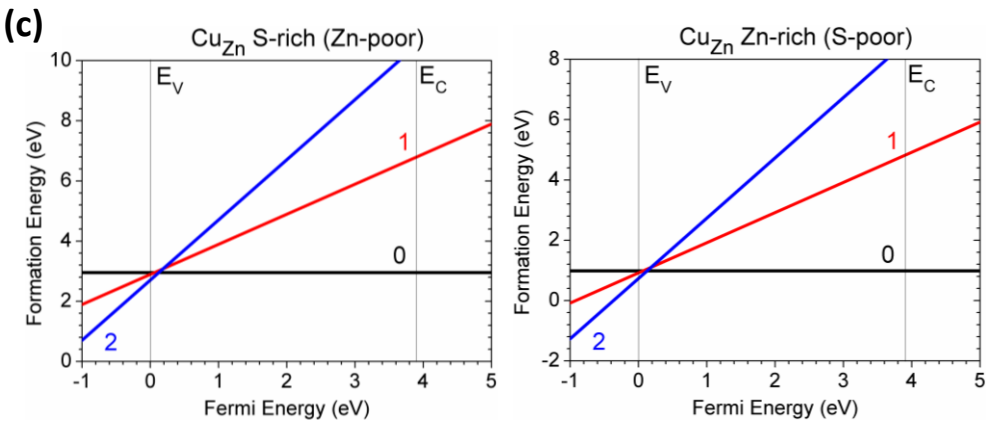

Figure 2. (a) PDOSs of Cu_{Zn} in neutral (Cu_{Zn}^{0}), singly positive (Cu_{Zn}^{+}), and doubly positively (Cu_{Zn}^{2+}). The dashed line denotes the highest occupied level for electrons. (b) Localized electron and hole orbitals at the relaxed Cu_{Zn} site (Zn=gray, O=red, S=yellow, Ca=green, Cu=Brown). (c) Formation energies of Cu_{Zn} under S and Zn rich chemical potential limits.

Figure 3.

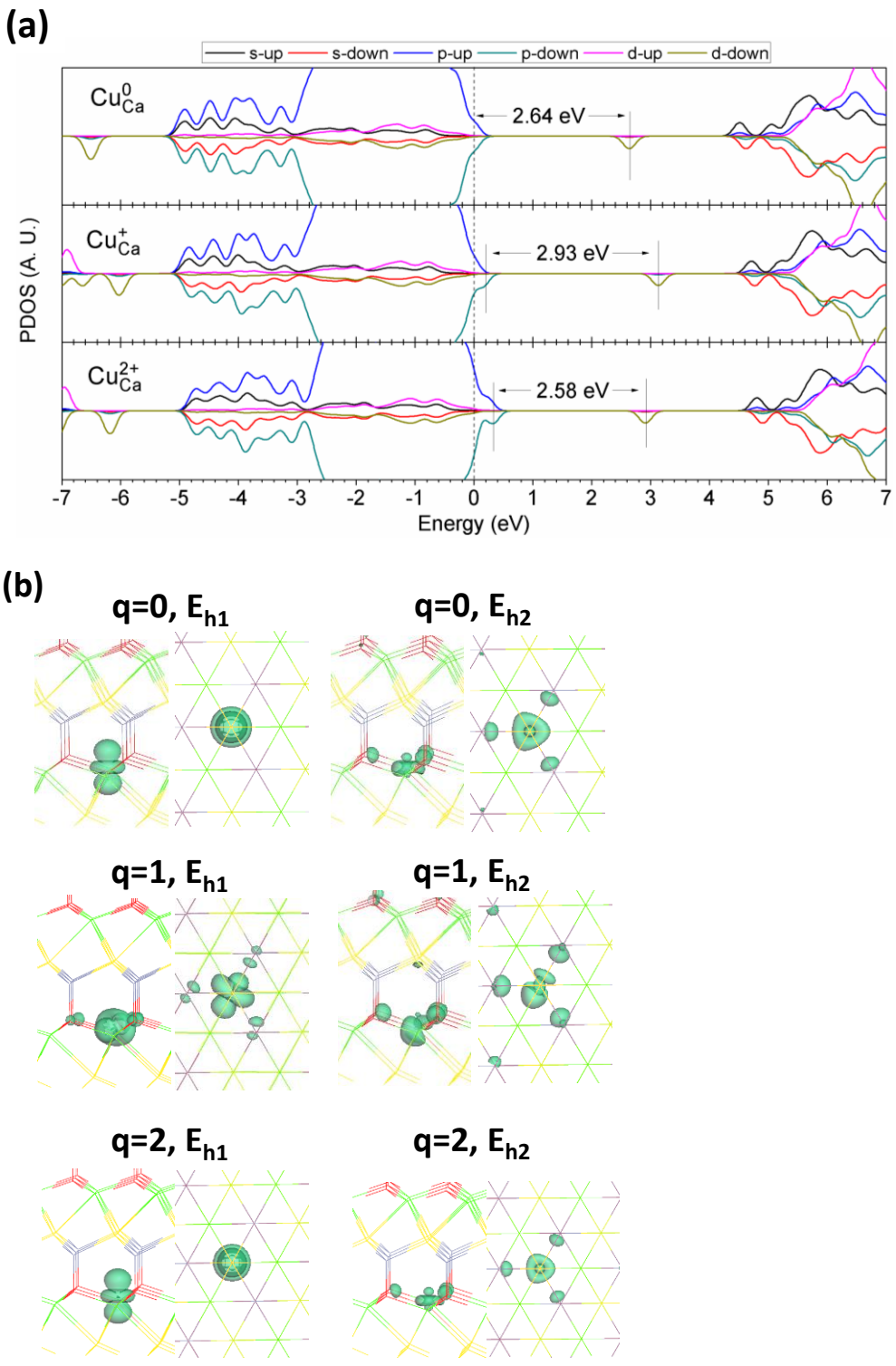
(a)
s-up
s-down
p-up
p-down
d-up
d-down
Cu^{0}_{Ca}
2.64 eV
Cu^{+}_{Ca}
2.93 eV
Cu^{2+}_{Ca}
2.58 eV
PDOS (A. U.)
-7 -6 -5 -4 -3 -2 -1 0 1 2 3 4 5 6 7
Energy (eV)
(b)
q=0, E_{h1}
q=0, E_{h2}
q=1, E_{h1}
q=1, E_{h2}
q=2, E_{h1}
q=2, E_{h2}

(c)

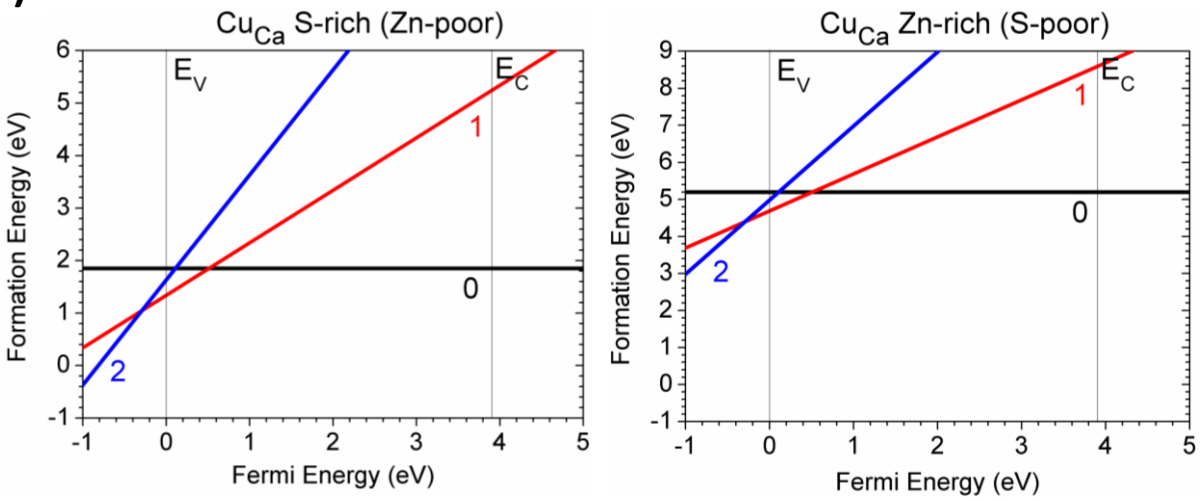

Figure 3. (a) PDOSs of Cu_{Ca} in neutral (Cu_{Ca}^{0}), singly positive (Cu_{Ca}^{+}), and doubly positively (Cu_{Ca}^{2+}). The dashed line denotes the highest occupied level for electrons. (b) Localized electron and hole orbitals at the relaxed Cu_{Ca} site (Zn=gray, O=red, S=yellow, Ca=green, Cu=Brown). (c) Formation energies of Cu_{Ca} under S and Zn rich chemical potential limits.

Figure 4.

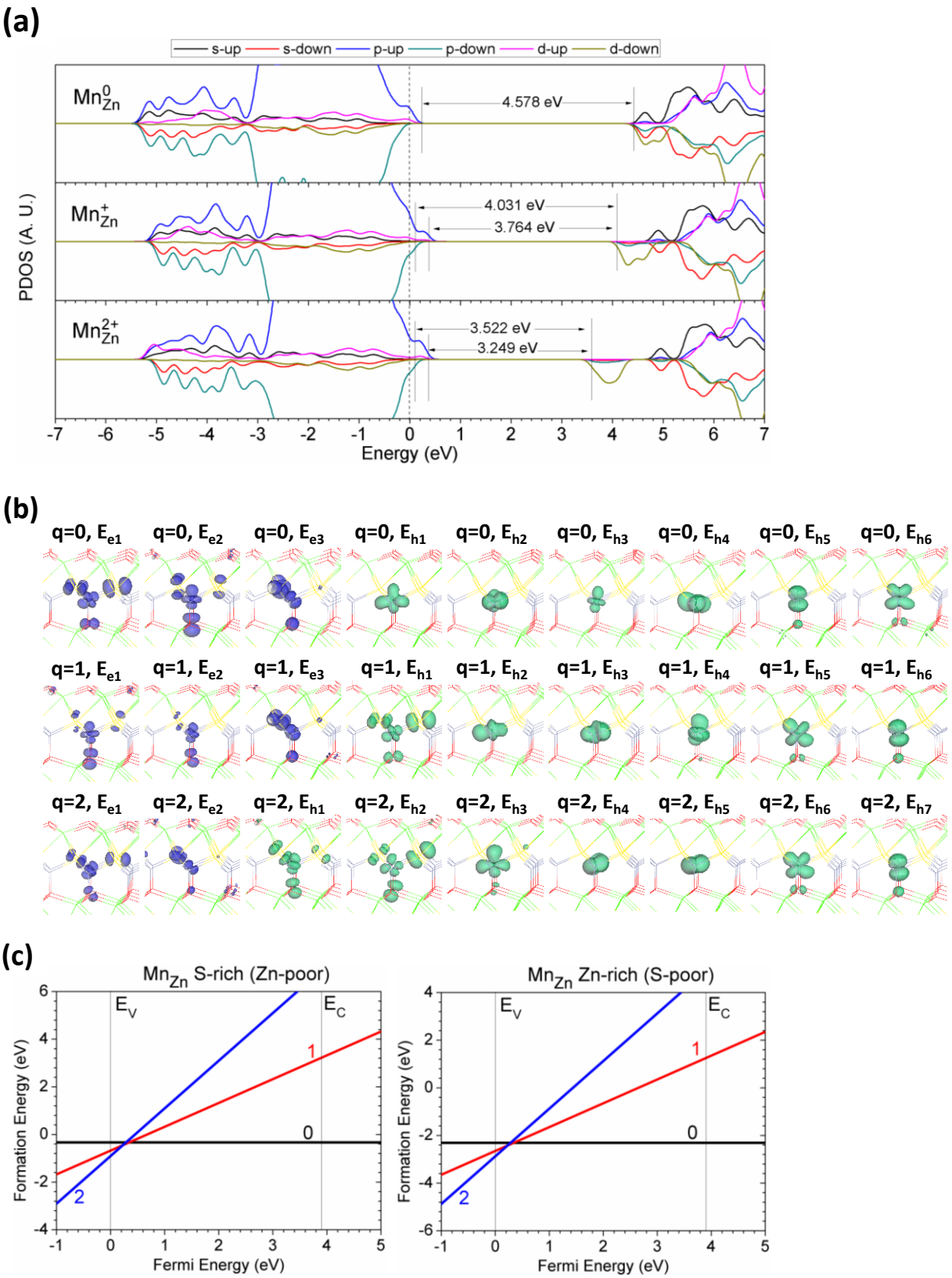
(a)
s-up
s-down
p-up
p-down
d-up
d-down
Mn^{0}_{Zn}
4.578 eV
Mn^{+}_{Zn}
4.031 eV
3.764 eV
Mn^{2+}_{Zn}
3.522 eV
3.249 eV
PDOS (A. U.)
Energy (eV)
(b)
q=0, E_{e1}
q=0, E_{e2}
q=0, E_{e3}
q=0, E_{h1}
q=0, E_{h2}
q=0, E_{h3}
q=0, E_{h4}
q=0, E_{h5}
q=0, E_{h6}
q=1, E_{e1}
q=1, E_{e2}
q=1, E_{e3}
q=1, E_{h1}
q=1, E_{h2}
q=1, E_{h3}
q=1, E_{h4}
q=1, E_{h5}
q=1, E_{h6}
q=2, E_{e1}
q=2, E_{e2}
q=2, E_{h1}
q=2, E_{h2}
q=2, E_{h3}
q=2, E_{h4}
q=2, E_{h5}
q=2, E_{h6}
q=2, E_{h7}
(c)
Mn_{Zn} S-rich (Zn-poor)
Mn_{Zn} Zn-rich (S-poor)
E_V
E_C
Formation Energy (eV)
Fermi Energy (eV)
0
1
2

Figure 4. (a) PDOSs of Mn_{Zn} in neutral (Mn_{Zn}^{0}), singly positive (Mn_{Zn}^{+}), and doubly positively (Mn_{Zn}^{2+}). The dashed line denotes the highest occupied level for electrons. (b) Localized electron and hole orbitals at the relaxed Mn_{Zn} site (Zn=gray, O=red, S=yellow, Ca=green, Cu=Brown). (c) Formation energies of Mn_{Zn} under S and Zn rich chemical potential limits.

Figure 5.

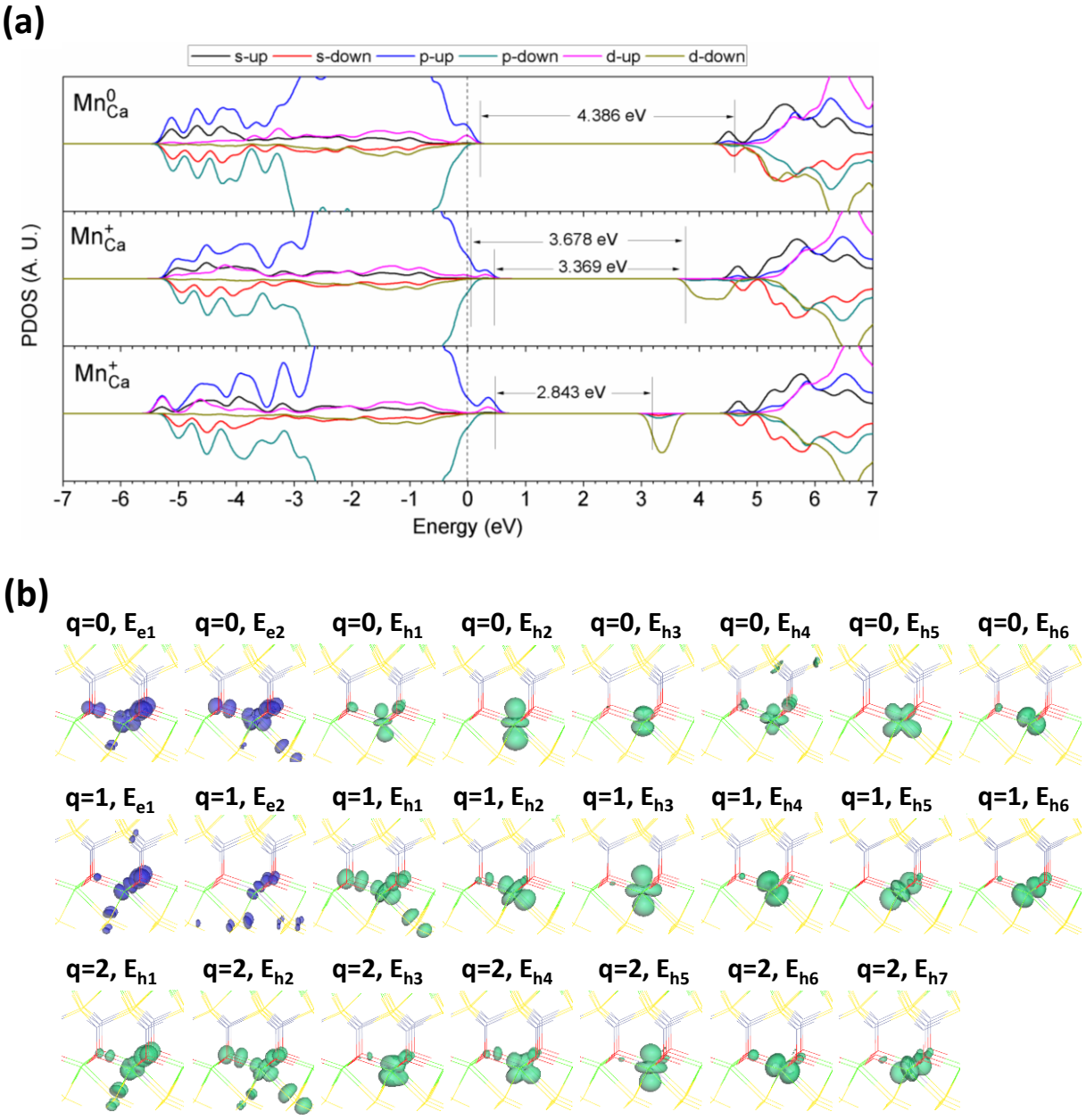
(a)
s-up
s-down
p-up
p-down
d-up
d-down
Mn^{0}_{Ca}
Mn^{+}_{Ca}
Mn^{+}_{Ca}
4.386 eV
3.678 eV
3.369 eV
2.843 eV
PDOS (A. U.)
Energy (eV)
(b)
q=0, E_{e1}
q=0, E_{e2}
q=0, E_{h1}
q=0, E_{h2}
q=0, E_{h3}
q=0, E_{h4}
q=0, E_{h5}
q=0, E_{h6}
q=1, E_{e1}
q=1, E_{e2}
q=1, E_{h1}
q=1, E_{h2}
q=1, E_{h3}
q=1, E_{h4}
q=1, E_{h5}
q=1, E_{h6}
q=2, E_{h1}
q=2, E_{h2}
q=2, E_{h3}
q=2, E_{h4}
q=2, E_{h5}
q=2, E_{h6}
q=2, E_{h7}

(c)

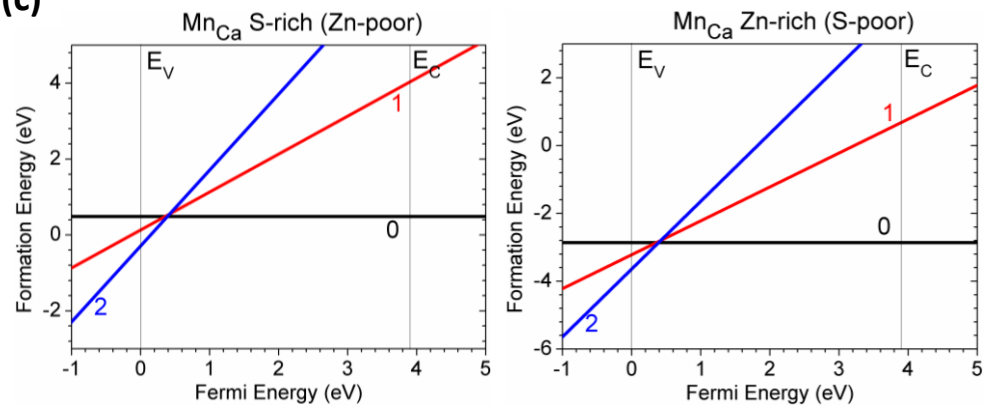

Figure 5. (a) PDOSs of Mn_{Ca} in neutral (Mn_{Ca}^{0}), singly positive (Mn_{Ca}^{+}), and doubly positively (Mn_{Ca}^{2+}). The dashed line denotes the highest occupied level for electrons. (b) Localized electron and hole orbitals at the relaxed Mn_{Ca} site (Zn=gray, O=red, S=yellow, Ca=green, Cu=Brown). (c) Formation energies of Mn_{Ca} under S and Zn rich chemical potential limits.

Figure 6.

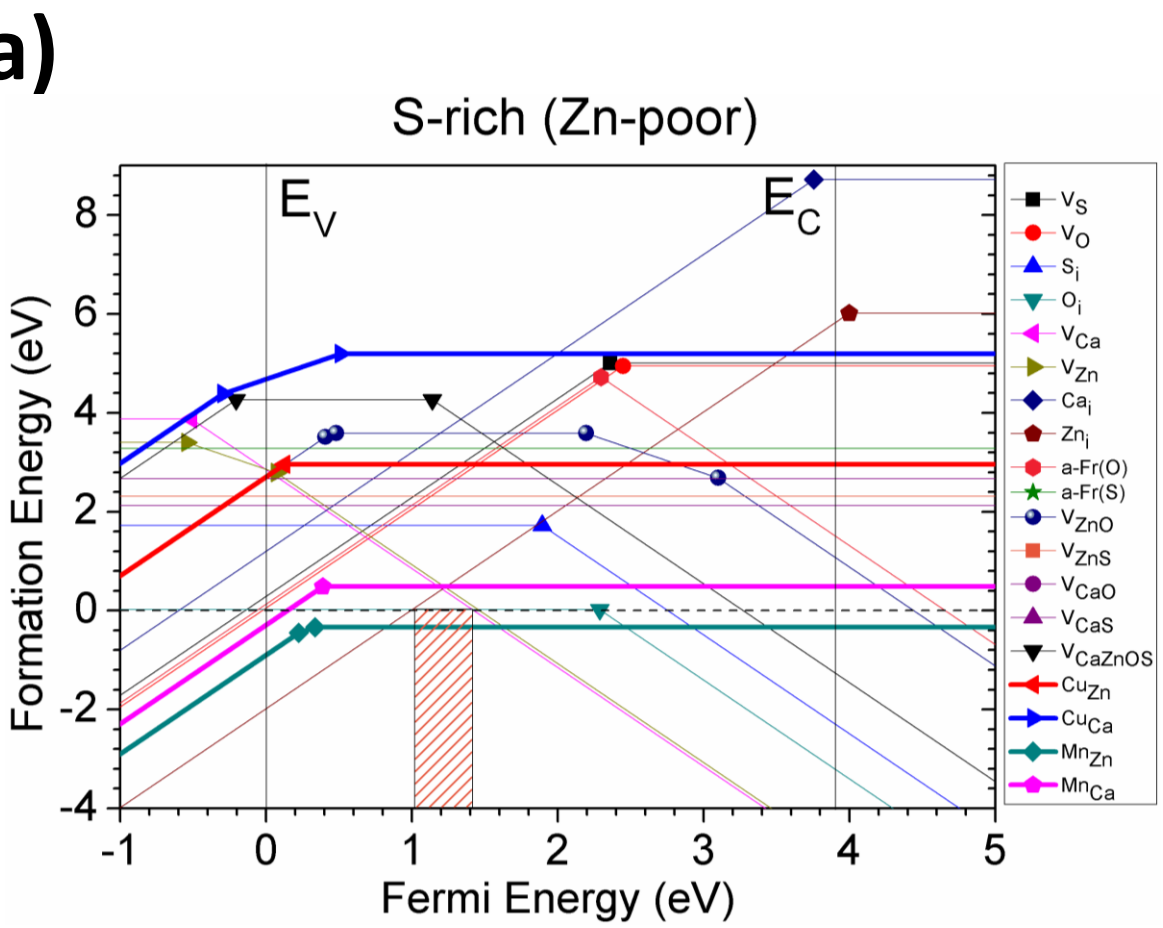
(a)
S-rich (Zn-poor)
E_V
E_C
Formation Energy (eV)
Fermi Energy (eV)
8
6
4
2
0
-2
-4
-1
0
1
2
3
4
5
V_S
V_O
S_i
O_i
V_Ca
V_Zn
Ca_i
Zn_i
a-Fr(O)
a-Fr(S)
V_ZnO
V_ZnS
V_CaO
V_CaS
V_CaZnOS
Cu_Zn
Cu_Ca
Mn_Zn
Mn_Ca

(b)

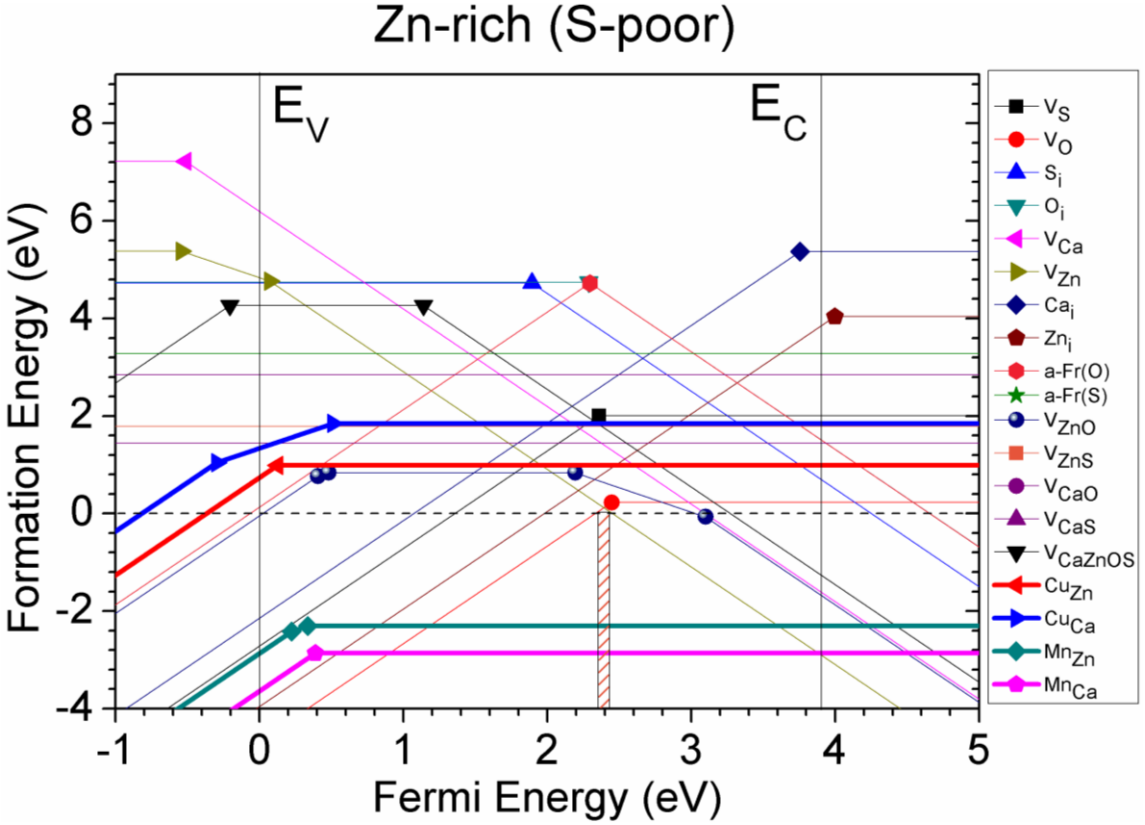

Figure 6. Summary of the native point defects in CaZnOS under S-rich (a) and Zn-rich (b) chemical potential limits, with consideration of the Cu (Cu_{Zn} and Cu_{Ca}) and Mn (Mn_{Zn} and Mn_{Ca}) doping. Orange shaded area denotes the dopable range for tuning the E_F positions that would not cause the spontaneous formation of native point defect or opposite charges for compensation.

Figure 7.

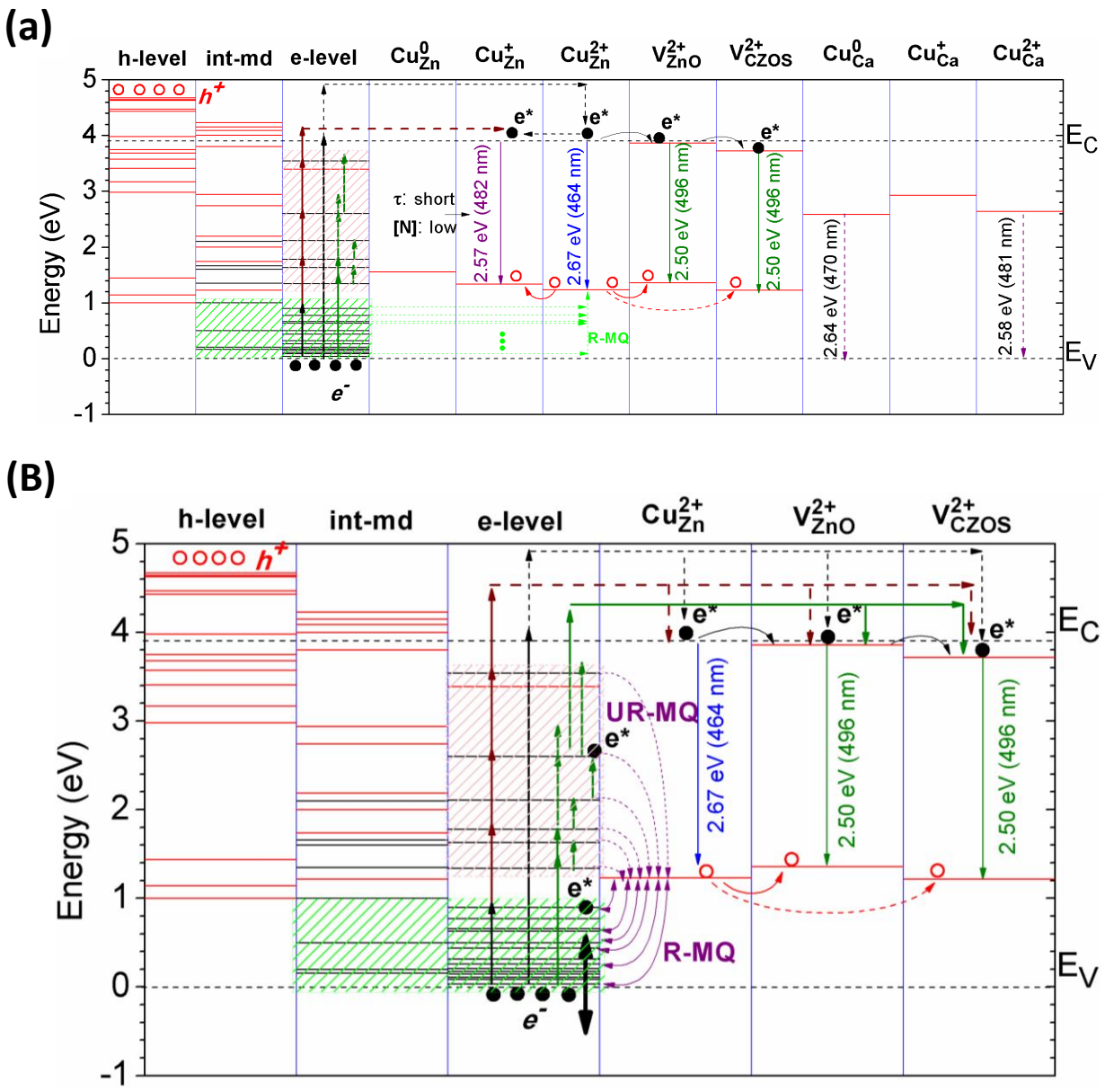
(a)
h-level
int-md
e-level
Cu^{0}_{Zn}
Cu^{+}_{Zn}
Cu^{2+}_{Zn}
V^{2+}_{ZnO}
V^{2+}_{CZOS}
Cu^{0}_{Ca}
Cu^{+}_{Ca}
Cu^{2+}_{Ca}
Energy (eV)
E_C
E_V
h+
e*
e-
τ: short
[N]: low
2.57 eV (482 nm)
2.67 eV (464 nm)
2.50 eV (496 nm)
2.50 eV (496 nm)
2.64 eV (470 nm)
2.58 eV (481 nm)
R-MQ
(B)
h-level
int-md
e-level
Cu^{2+}_{Zn}
V^{2+}_{ZnO}
V^{2+}_{CZOS}
Energy (eV)
E_C
E_V
h+
e*
e-
UR-MQ
R-MQ
2.67 eV (464 nm)
2.50 eV (496 nm)
2.50 eV (496 nm)

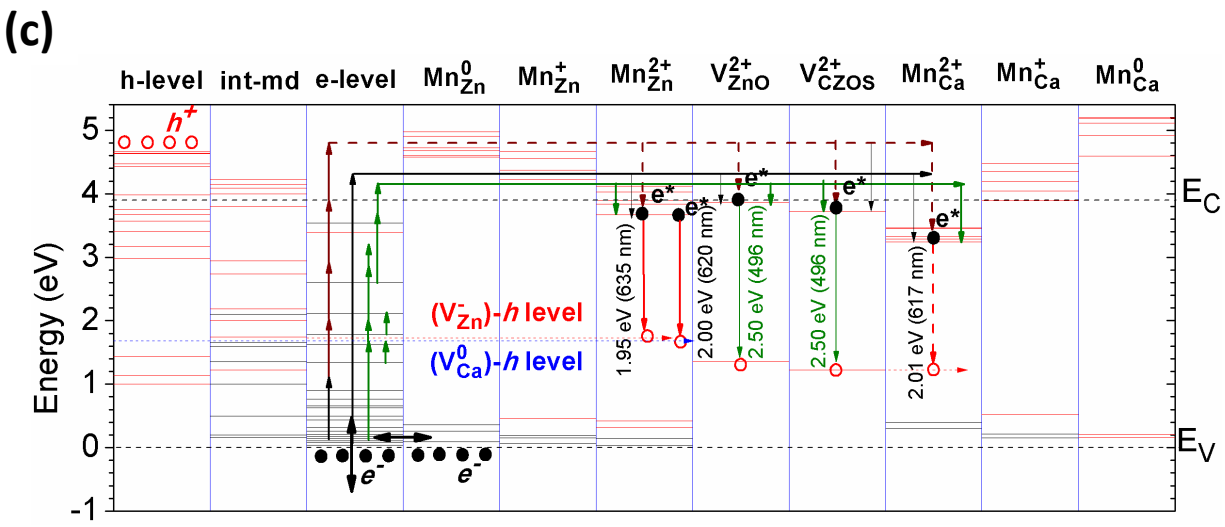

Figure 7. (a) Summarized single-particle levels of intrinsic defects in CaZnOS with different charge states (empty states=red, filled states=black) and the related Cu_{Zn} and Cu_{Ca} doping levels. (b) Summarized energy diagram for illustrating the mechanism of reversible mechanical quenching (R-MQ) and un-reversible mechanical quenching (UR-MQ) effects of Cu doped luminescence process. (c) Summarized single-particle levels of intrinsic defects in CaZnOS with different charge states (empty states=red, filled states=black) and the related Mn_{Zn} and Mn_{Ca} doping levels.

Figure 8.

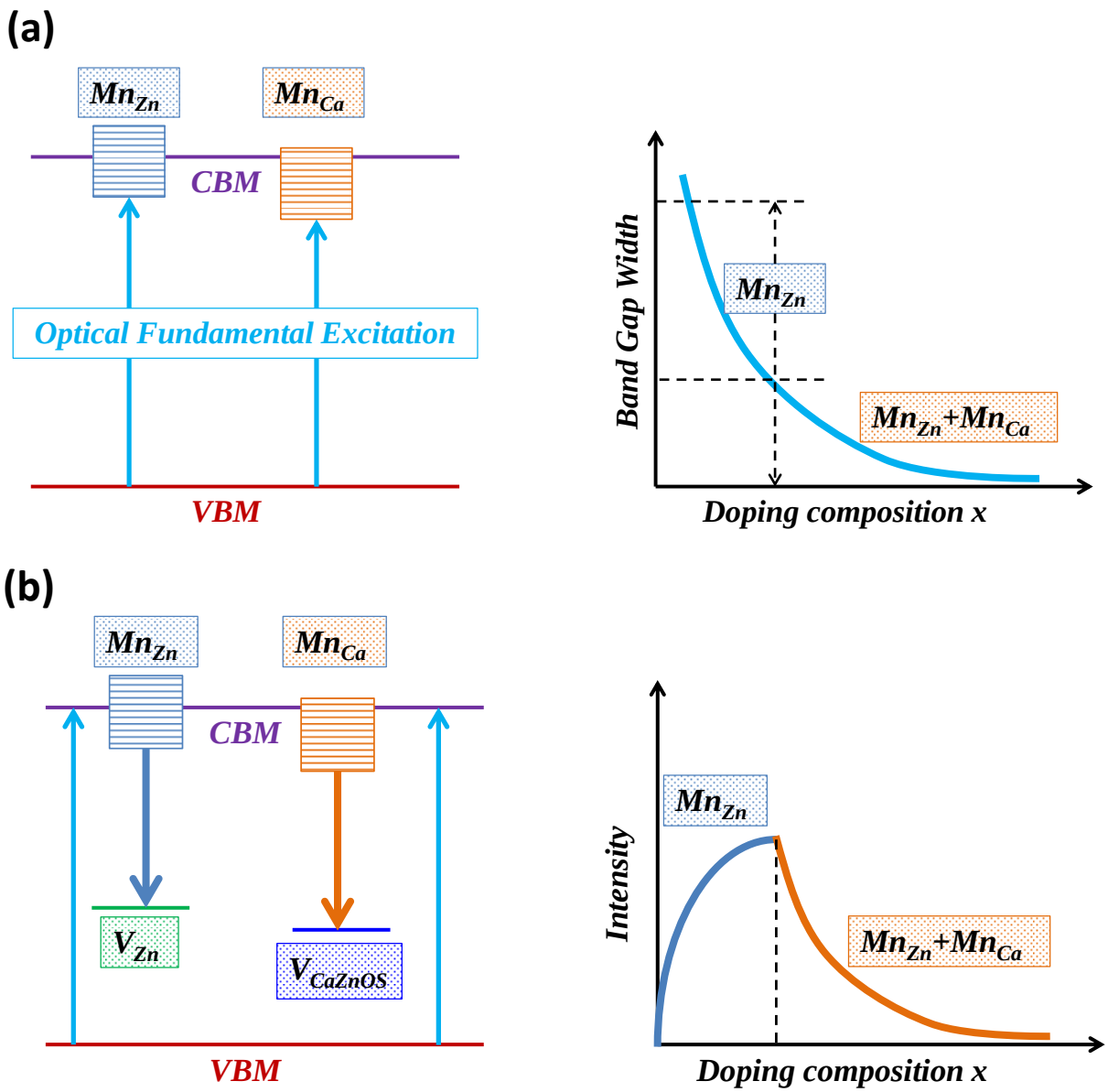
(a)
Mn_{Zn}
Mn_{Ca}
CBM
Optical Fundamental Excitation
VBM
Band Gap Width
Mn_{Zn}
Mn_{Zn}+Mn_{Ca}
Doping composition x
(b)
Mn_{Zn}
Mn_{Ca}
CBM
V_{Zn}
V_{CaZnOS}
VBM
Intensity
Mn_{Zn}
Mn_{Zn}+Mn_{Ca}
Doping composition x

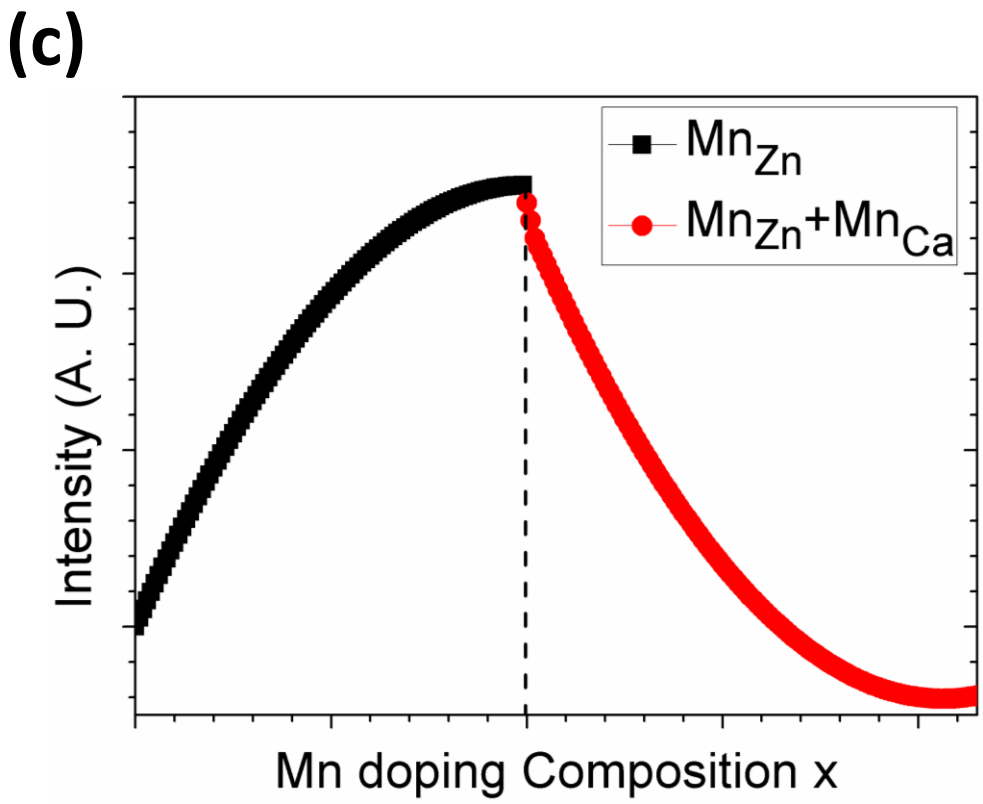

Figure 8. (a) Schematic diagram to illustrate the band gap width dependent on the Mn doping concentration due to the absorption edge red-shifted. (b) Schematic diagram with analysis model to demonstrate the Mn-doping concentration quenching effect. (c) Numerical fitting model to model the diagram in (b).

References

[1] Z. L. Wang, Nano Today **5**, 540 (2010).
[2] W. Wu and Z. L. Wang, Nature Reviews Materials, 16031 (2016).
[3] X. Wang, et al., Adv. Mater. **27**, 2324 (2015).
[4] D. Peng, B. Chen, and F. Wang, Chempluschem **80**, 1209 (2015).
[5] D. Tu, C.-N. Xu, Y. Fujio, and A. Yoshida, Light Sci Appl **4**, e356 (2015).
[6] H. Zhang, D. Peng, W. Wang, L. Dong, and C. Pan, J. Phys. Chem. C **119**, 28136 (2015).
[7] Y. Zhang, G. Gao, H. L. W. Chan, J. Dai, Y. Wang, and J. Hao, Adv. Mater. **24**, 1729 (2012).
[8] M.-C. Wong, L. Chen, M.-K. Tsang, Y. Zhang, and J. Hao, Adv. Mater. **27**, 4488 (2015).
[9] L.-B. Huang, G. Bai, M.-C. Wong, Z. Yang, W. Xu, and J. Hao, Adv. Mater. **28**, 2744 (2016).
[10] T. Aitasalo, P. Dereń, J. Hölsä, H. Jungner, J. C. Krupa, M. Lastusaari, J. Legendziewicz, J. Niittykoski, and W. Stręk, J. Solid State Chem. **171**, 114 (2003).
[11] T. Matsuzawa, Y. Aoki, N. Takeuchi, and Y. Murayama, J. Electrochem. Soc. **143**, 2670 (1996).
[12] K. Van den Eeckhout, P. F. Smet, and D. Poelman, Materials **3**, 2536 (2010).
[13] K. Van den Eeckhout, D. Poelman, and P. Smet, Materials **6**, 2789 (2013).
[14] Z. Pan, Y.-Y. Lu, and F. Liu, Nat Mater **11**, 58 (2012).
[15] T. Maldiney, et al., Nat Mater **13**, 418 (2014).
[16] A. Abdukayum, J.-T. Chen, Q. Zhao, and X.-P. Yan, J. Am. Chem. Soc. **135**, 14125 (2013).
[17] Z. Li, Y. Zhang, X. Wu, L. Huang, D. Li, W. Fan, and G. Han, J. Am. Chem. Soc. **137**, 5304 (2015).
[18] D. C. Rodriguez Burbano, E. M. Rodriguez, P. Dorenbos, M. Bettinelli, and J. A. Capobianco, Journal of Materials Chemistry C **2**, 228 (2014).
[19] D. C. Rodríguez Burbano, S. K. Sharma, P. Dorenbos, B. Viana, and J. A. Capobianco, Advanced Optical Materials **3**, 551 (2015).
[20] G.-y. Adachi and N. Imanaka, Chem. Rev. **98**, 1479 (1998).
[21] P. F. Smet, I. Moreels, Z. Hens, and D. Poelman, Materials **3**, 2834 (2010).
[22] P. Gluchowski, W. Strek, M. Lastusaari, and J. Holsa, Phys. Chem. Chem. Phys. **17**, 17246 (2015).
[23] T.-W. Kuo, W.-R. Liu, and T.-M. Chen, Opt. Express **18**, 8187 (2010).
[24] F. Auzel, Chem. Rev. **104**, 139 (2004).
[25] L.-D. Sun, Y.-F. Wang, and C.-H. Yan, Accounts. Chem. Res. **47**, 1001 (2014).
[26] X. Liu, C.-H. Yan, and J. A. Capobianco, Chem. Soc. Rev. **44**, 1299 (2015).
[27] L.-D. Sun, H. Dong, P.-Z. Zhang, and C.-H. Yan, Annu. Rev. Phys. Chem. **66**, 619 (2015).
[28] H. Dong, L.-D. Sun, and C.-H. Yan, Chem. Soc. Rev. **44**, 1608 (2015).
[29] Z.-J. Zhang, A. Feng, X.-Y. Chen, and J.-T. Zhao, J. Appl. Phys. **114**, 213518 (2013).
[30] B. Huang, Phys. Chem. Chem. Phys. **18**, 25946 (2016).
[31] J. Hölsä, Electrochem. Soc. Interf. **18**, 42 (2009).
[32] J.-C. Zhang, C.-N. Xu, S. Kamimura, Y. Terasawa, H. Yamada, and X. Wang, Opt. Express **21**, 12976 (2013).
[33] J.-C. Zhang, L.-Z. Zhao, Y.-Z. Long, H.-D. Zhang, B. Sun, W.-P. Han, X. Yan, and X. Wang, Chem. Mater. **27**, 7481 (2015).

[34] B. Huang, Inorg. Chem. **54**, 11423 (2015).
[35] B. Huang, Phys. Chem. Chem. Phys. **18**, 13564 (2016).
[36] B. Huang, R. Gillen, and J. Robertson, J. Phys. Chem. C **118**, 24248 (2014).
[37] B. Huang, Philosophical Magazine **94**, 3052 (2014).
[38] B. Huang and J. Robertson, Phys. Rev. B **85**, 125305 (2012).
[39] B. Huang and J. Robertson, J. Non-cryst. Solids. **358**, 2393 (2012).
[40] B. Huang, physica status solidi (b) **252**, 431 (2015).
[41] A. De Vos, K. Lejaeghere, D. E. P. Vanpoucke, J. J. Joos, P. F. Smet, and K. Hemelsoet, Inorg. Chem. **55**, 2402 (2016).
[42] B. Qu, B. Zhang, L. Wang, R. Zhou, and X. C. Zeng, Chem. Mater. **27**, 2195 (2015).
[43] C. J. Duan, A. C. A. Delsing, and H. T. Hintzen, Chem. Mater. **21**, 1010 (2009).
[44] P. Li, S. Deng, L. Zhang, G. Liu, and J. Yu, Chem. Phys. Lett. **531**, 75 (2012).
[45] S. J. Clark, J. Robertson, S. Lany, and A. Zunger, Phys. Rev. B **81**, 115311 (2010).
[46] A. Janotti and C. G. Van de Walle, Phys. Rev. B **76**, 165202 (2007).
[47] S. J. Clark, M. D. Segall, C. J. Pickard, P. J. Hasnip, M. I. J. Probert, K. Refson, and M. C. Payne, Zeitschrift Fur Kristallographie **220**, 567 (2005).
[48] N. Marzari, D. Vanderbilt, and M. C. Payne, Phys. Rev. Lett. **79**, 1337 (1997).
[49] M. I. J. Probert and M. C. Payne, Phys. Rev. B **67**, 075204 (2003).
[50] I. A. Vladimir, F. Aryasetiawan, and A. I. Lichtenstein, J. Phys.: Condens. Matter **9**, 767 (1997).
[51] C. J. Pickard, B. Winkler, R. K. Chen, M. C. Payne, M. H. Lee, J. S. Lin, J. A. White, V. Milman, and D. Vanderbilt, Phys. Rev. Lett. **85**, 5122 (2000).
[52] B. Huang, Solid State Commun. **230**, 49 (2016).
[53] B. Huang, Solid State Commun. **237–238**, 34 (2016).
[54] B. Huang, J. Comput. Chem. **37**, 825 (2016).
[55] B. Huang, H. Dong, K.-L. Wong, L.-D. Sun, and C.-H. Yan, J. Phys. Chem. C **120**, 18858 (2016).
[56] S. Lany and A. Zunger, Phys. Rev. B **80**, 085202 (2009).
[57] S. Lany and A. Zunger, Phys. Rev. B **81**, 205209 (2010).
[58] B. J. Morgan and G. W. Watson, J. Phys. Chem. C **114**, 2321 (2010).
[59] P. R. L. Keating, D. O. Scanlon, B. J. Morgan, N. M. Galea, and G. W. Watson, J. Phys. Chem. C **116**, 2443 (2011).
[60] A. M. Rappe, K. M. Rabe, E. Kaxiras, and J. D. Joannopoulos, Phys. Rev. B **41**, 1227 (1990).
[61] L. Kleinman and D. M. Bylander, Phys. Rev. Lett. **48**, 1425 (1982).
[62] S. G. Louie, S. Froyen, and M. L. Cohen, Phys. Rev. B **26**, 1738 (1982).
[63] S. Lany and A. Zunger, Phys. Rev. B **78**, 235104 (2008).
[64] P. Tanner, in *Lanthanide Luminescence*, edited by P. Hänninen and H. Härmä (Springer Berlin Heidelberg, 2011), Vol. 7, p. 183.
[65] S. Lany and A. Zunger, Phys. Rev. Lett. **93**, 156404 (2004).
[66] S. Lany and A. Zunger, Phys. Rev. B **72**, 035215 (2005).
[67] Z. Qiu, C. Rong, W. Zhou, J. Zhang, C. Li, L. Yu, S. Liu, and S. Lian, Journal Of Alloys and Compounds **583**, 335 (2014).